








Dynamical architecture of the HD 107148 system

JAN EBERHARDT ¹, TRIFON TRIFONOV ¹, MARTIN KÜRSTER ¹, STEPHAN STOCK ², THOMAS HENNING ¹,
ANNA WOLLBOLD¹, SABINE REFFERT ², MAN HOI LEE ^{3,4}, MATHIAS ZECHMEISTER ⁵, FLORIAN RODLER ⁶,
OLGA ZAKHOZHAY ^{1,7}, PAUL HEEREN ², DAVIDE GANDOLFI ⁸, OSCAR BARRAGÁN ⁹, MARCELO TALA PINTO ¹⁰,
VERA WOLTHOFF², PAULA SARKIS ¹ AND STEFAN S. BREMS ²

¹Max-Planck-Institut für Astronomie, Königstuhl 17, 69117 Heidelberg, Germany

²Landessternwarte, Zentrum für Astronomie der Universität Heidelberg, Königstuhl 12, 69117 Heidelberg, Germany

³Department of Earth Sciences, The University of Hong Kong, Pokfulam Road, Hong Kong

⁴Department of Physics, The University of Hong Kong, Pokfulam Road, Hong Kong

⁵Institut für Astrophysik, Georg-August-Universität, Friedrich-Hund-Platz 1, 37077 Göttingen, Germany

⁶European Southern Observatory (ESO), Alonso de Cordova 3107, Vitacura, Santiago de Chile, Chile

⁷Main Astronomical Observatory, National Academy of Sciences of Ukraine, Kyiv 03143, Ukraine

⁸Dipartimento di Fisica, Università di Torino, via P. Giuria 1, 10125 Torino, Italy

⁹Sub-department of Astrophysics, Department of Physics, University of Oxford, Oxford OX1 3RH, UK

¹⁰Facultad de Ingeniería y Ciencias, Universidad Adolfo Ibáñez, Av. Diagonal las Torres 2640, Peñalolen, Santiago, Chile

ABSTRACT

We present an independent Doppler validation and dynamical orbital analysis of the two-planet system HD 107148, which was recently announced in Rosenthal et al. (2021). Our detailed analyses are based on literature HIRES data and newly obtained HARPS and CARMENES radial velocity (RV) measurements as part of our survey in search for additional planets around single planet systems. We perform a periodogram analysis of the available HIRES and HARPS precise RVs and stellar activity indicators. We do not find any apparent correlation between the RV measurements and the stellar activity indicators, thus linking the two strong periodicities to a moderately compact multiple-planet system. We carry out orbital fitting analysis by testing various one- and two-planet orbital configurations and studying the posterior probability distribution of the fitted parameters. Our results solidify the existence of a Saturn-mass planet (HD 107148 b, discovered first) with a period $P_b \sim 77.2$ d, and a second, eccentric ($e_c \sim 0.4$), Neptune-mass exoplanet (HD 107148 c), with an orbital period of $P_c \sim 18.3$ d. Finally, we investigate the two-planet system's long-term stability and overall orbital dynamics with the posterior distribution of our preferred orbital configuration. Our N-body stability simulations show that the system is long-term stable and exhibits large secular osculations in eccentricity but in no particular mean-motion resonance configuration. The HD 107148 system, consisting of a Solar-type main sequence star with two giant planets in a rare configuration, features a common proper motion white dwarf companion and is, therefore, a valuable target for understanding the formation and evolution of planetary systems.

Keywords: Exoplanet astronomy, Exoplanet detection methods, Radial velocity, Exoplanet dynamics, Exoplanet systems

1. INTRODUCTION

As of November 2021, there are more than 4800 known extrasolar planets (exoplanets), of which over 900 have been discovered with the radial velocity (RV) method utilizing the Doppler effect¹. The Doppler spectroscopy remains the best way for astronomers to determine the

exoplanet orbital geometry, eccentricity, and planetary mass distribution, which are fundamentally important for understanding planet formation and evolution. In radial velocity surveys for extrasolar planets, sparse phase coverage of the orbit may lead to model ambiguity, such that two near-resonant companions can mask as a single one in an eccentric orbit (see Anglada-Escudé et al. 2010; Wittenmyer et al. 2013; Kürster et al. 2015; Boisvert et al. 2018). With steadily improving instru-

¹ up to date statistics available at <http://exoplanet.eu>

ments, data analysis methods, and more precise data, it is worthwhile revisiting targets with already known planetary systems, as these could reveal additional undetected planets (see, e.g. [Marcy et al. 2001](#); [Trifonov et al. 2017](#); [Wittenmyer et al. 2019](#)).

We initiated an RV follow-up survey of single exoplanet systems discovered with the Doppler method, targeting systems announced to have exoplanets in moderately eccentric orbits based on relatively sparse RV datasets, for which an alternative multi-planet model cannot be excluded ([Kürster et al. 2015](#)). Our survey aims to obtain more precise RVs at critical orbital phases and re-analyze the orbital configuration looking for evidence of additional planets. Of particular interest to us are multi-planetary systems in low-order mean motion resonance (MMR), such as GJ 876 ([Marcy et al. 2001](#); [Rivera et al. 2010](#); [Trifonov et al. 2018](#)), HD 82943 ([Tan et al. 2013](#)), η Ceti ([Trifonov et al. 2014](#)), and other massive pairs (see, e.g., [Trifonov et al. 2019](#)). The strongly resonant architecture of such multi-planetary systems speaks in favor of planet migration, which makes their dynamical characteristics important elements for a comprehensive understanding of planet formation.

We present a new orbital analysis of the known planetary system around the G-dwarf star HD 107148, using archival Keck HIRES ([Vogt et al. 1994](#)) and newly obtained high-precision HARPS ([Mayor et al. 2003](#)) data. We find that our orbital period for HD 107148 b of $P_b \sim 77$ d differs significantly from the literature value of ~ 48 d, which we attribute to an alias induced from the HIRES observational schedule. We further find significant evidence for the existence of a second warm Neptune mass planet on an eccentric orbit ($e_c = 0.41$) with an orbital period of ~ 18 d. We present a detailed orbital update of the now confirmed two-planet system.

The paper is organized as follows; In [Sect. 2](#), we present an overview of the literature of the system. In [Sect. 3](#), we present the data we use for our analysis. [Sect. 4](#) describes our analysis methods and numerical setups and presents our main results. Summary and conclusions of our results are given in [Sect. 5](#).

2. THE HD 107148 SYSTEM

2.1. Stellar parameters

Literature stellar parameters and their $1\text{-}\sigma$ uncertainties for HD 107148 (HIP 60081, BD-02 3497, TIC 66666079), are listed in [Table 1](#). Briefly, HD 107148 is a Solar-type star with a stellar mass $M_\star = 1.127^{+0.035}_{-0.025} M_\odot$ and stellar radius $R_\star = 1.15 \pm 0.05 R_\odot$ ([Soto & Jenkins 2018](#)). In addition to age, mass, radius, and effective temperature, [Soto & Jenkins \(2018\)](#)

Table 1. Stellar parameters of HD 107148 and, if available, their $1\text{-}\sigma$ uncertainties.

Parameter	HD 107148	reference
Spectral type	G1V	[1]
V [mag]	8.01	[2]
$B - V$ [mag]	0.71	[2]
Distance [pc]	$49.486^{+0.115}_{-0.115}$	[3]
	$49.416^{+0.116}_{-0.115}$	[4]
Luminosity [L_\odot]	1.321	[4]
T_{eff} [K]	5833 ± 34	[5]
$\log g$ [cm s^{-2}]	4.42 ± 0.24	[5]
[Fe/H]	0.34 ± 0.07	[5]
Mass [M_\odot]	$1.127^{+0.035}_{-0.025}$	[5]
Radius [R_\odot]	$1.15^{+0.05}_{-0.05}$	[5]
Age [Gyr]	$3.5^{+1.5}_{-1.3}$	[5]
$v \sin i$ [km s^{-1}]	1.36 ± 0.210	[5]
Parallax [mas]	20.25 ± 0.03	[6]

NOTE—1 – determined according to [Pecaut & Mamajek \(2013\)](#), 2 – [ESA \(1997\)](#), 3 – [Gaia Collaboration et al. \(2018\)](#), 4 – [Bailer-Jones et al. \(2018\)](#), 5 – [Soto & Jenkins \(2018\)](#), 6 – [Gaia Collaboration et al. \(2021\)](#)

determined that HD 107148 is a super metal-rich star with $[\text{Fe}/\text{H}] = 0.34 \pm 0.07$. Precise parallax data obtained from the *Gaia* mission ([Gaia Collaboration et al. 2016, 2018](#)), indicate that HD 107148 is relatively close to the Sun with an estimated distance of $d = 49.486 \pm 0.115$ pc.

[Tokovinin & Lépine \(2012\)](#) reported the possible detection of a white dwarf (WD) stellar companion with a projected separation of about 1790 au from the main sequence star HD 107148. Later, [Mugrauer et al. \(2014\)](#) confirmed the WD companion as HD 107148 B (we continue to call the main sequence star HD 107148 without adding an extra "A"). For the WD companion [Mugrauer & Dinçel \(2016\)](#) obtained a mass of $M_{WD} = 0.56 \pm 0.05 M_\odot$, an effective temperature of $T_{\text{eff}} = 6150 \pm 250$ K, a cooling age of 2.1 ± 0.27 Gyr, a surface gravity of $\log g = 7.95 \pm 0.09 \text{ cm s}^{-2}$ and a luminosity of $L = (2.0 \pm 0.2) \times 10^{-4} L_\odot$. By assuming the initial-to-final-mass-relation for white dwarfs from [Catalan et al. \(2008\)](#), [Mugrauer & Dinçel \(2016\)](#) derived a progenitor mass of $1.4 \pm 0.6 M_\odot$, leading to an estimated total age of 6.0 ± 4.8 Gyr for the WD companion.

2.2. Literature overview of the exoplanet system

Based on 35 Keck HIRES observations, obtained over a temporal baseline of six years (January 2000 to January 2006), [Butler et al. \(2006\)](#) reported the discovery of an exoplanet companion, HD 107148 b, with an or-

bital period of $P = 48.056 \pm 0.057$ d, eccentricity of $e = 0.05 \pm 0.17$ and a mass of $m \sin i = 0.210 \pm 0.036 M_{\text{jup}}$. Later, with more HIRES data available (a total 60 observations from January 2000 to January 2014), [Butler et al. \(2017\)](#) reported a significant periodicity in HD 107148 b of $P = 77.26 \pm 0.09$ d², which does not match their earlier result of 48 d. In this work, we show that the signal of ~ 48 d is an alias of the true planetary period of HD 107148 b, which is successfully recovered by [Butler et al. \(2017\)](#) and our work, using more HIRES and HARPS data (see [Sect. 4.1](#)).

HD 107148 has been observed as part of campaign 10 of the Kepler K2 mission ([Howell et al. 2014](#)). Our inspection of the light curves did not reveal any planetary transit signal. During the revision of this paper, we become aware that HD 107148 was observed by the Transiting Exoplanet Survey Satellite (TESS, [Ricker et al. 2015](#)) in sector 46. We inspected the light curve and found no transit signal in the TESS photometry window. Further, we found the TESS light curve stable over sector 46, suggesting that HD 107148 is likely a photometrically quiet star.

During the advanced stage of this work, we became aware of the results from the *The California Legacy Survey* ([Rosenthal et al. 2021](#); [Fulton et al. 2021](#)), which includes HD 107148. In particular, [Rosenthal et al. \(2021\)](#) present an updated orbital catalog of 178 planets, based on a large collection of RVs obtained with the Keck-HIRES ([Vogt et al. 1994](#)), APF-Levy ([Vogt et al. 2014](#)), and Lick-Hamilton ([Fischer et al. 2013](#)) spectrographs over the past three decades. In their paper, they correctly identified the frequency of ~ 48 d as an alias of the actual period of HD 107148 b (~ 77 d), and also reported evidence of a new Neptune-mass planet with a period of $P_c \sim 18.33$ d, which is in excellent agreement with our conclusions reported in this work. Our work differs from that of [Rosenthal et al. \(2021\)](#) in that we also perform a detailed orbital, activity, and dynamical analysis of the system. Also the orbital update reported in [Rosenthal et al. \(2021\)](#) is based on old and newly obtained proprietary HIRES RVs, whereas our independent discovery of HD 107148 c is based on newly obtained HARPS data in addition to the literature HIRES data set from [Butler et al. \(2017\)](#). We consider the independent work of both teams and their mutually agreeing results to be solid evidence of the existence of the HD 107148 b & c planets.

3. DATA

3.1. HIRES data

We found 60 precise RV measurements of HD 107148 obtained with the High Resolution Échelle Spectrograph, mounted to the 10-m telescope of Keck Observatory, Hawaii, USA, (HIRES, [Vogt et al. 1994](#)). HIRES is a general-purpose spectrograph, which relies on the iodine (I₂) cell technique ([Marcy & Butler 1992](#)) to achieve radial velocity measurements with a precision of about 3 m s^{-1} ([Butler et al. 1996](#)).

The HIRES RV data of HD 107148 were made publicly available in the [Butler et al. \(2017\)](#) catalog of precise Doppler measurements and stellar-line activity-index measurements, which consists of $\sim 65\,000$ HIRES spectra for ~ 1700 stars obtained between 1996 and 2014. Shortly after [Butler et al. \(2017\)](#) published their RV collection, [Tal-Or et al. \(2019\)](#) re-analyzed and corrected the HIRES data set for small yet significant systematic nightly zero-point variations in the data, increasing the precision. The magnitude of these corrections is of the order of $\sim 1 \text{ m s}^{-1}$ and does not strongly affect our orbital analysis, yet we decided to use the more precise RV data set released by [Tal-Or et al. \(2019\)](#). From these data, we omitted one outlier taken at epoch BJD = 2451704.828, by performing a $3\text{-}\sigma$ -clipping to the HIRES data set.

The HIRES data were obtained between January 2000 and January 2014 with a total temporal baseline of 5122 d and have a weighted root mean square of $\text{WRMS}_{\text{HIRES}} = 6.7 \text{ m s}^{-1}$ and a median RV uncertainty of $\hat{\sigma}_{\text{HIRES}} = 1.5 \text{ m s}^{-1}$, respectively.

3.2. HARPS data

We obtained a total of 92 high signal-to-noise spectra of HD 107148 with the High Accuracy Radial velocity Planet Searcher spectrograph (HARPS [Mayor et al. 2003](#)), mounted at the ESO 3.6 m Telescope, La Silla, Chile. We also found a total of 13 archival HARPS spectra of HD 107148 in the official ESO archive³. Thus, for HD 107148, we have a total of 105 HARPS spectra from which we extracted high-precision RVs for our orbital analysis.

We derived precise RV measurements and spectral activity indices with the SpEctrum Radial Velocity AnaLyser (SERVAL, [Zechmeister et al. 2018](#)) pipeline, as well as with the official HARPS-DRS pipeline. From SERVAL we obtained the time series of the stellar activity indicators chromatic index (CRX), differential line width (dLW), H α , and Na D₁ and D₂ (see [Zechmeister et al. 2018](#), for more details), whereas from the DRS,

² This value does not appear in recent databases, but appears in the supplementary Table 2 of [Butler et al. \(2017\)](#)

³ http://archive.eso.org/wdb/wdb/adp/phase3_main/form

we obtained the cross-correlation function (CCF), full width half maximum FWHM, the CCF Bisector slope (BIS), and contrast (CON), which are important stellar activity indices (e.g. Queloz et al. 2001). We note that in May 2015, the HARPS spectrograph underwent a major upgrade of the fiber link between the telescope focal plane and the spectrograph entrance (see, Lo Curto et al. 2015). This resulted in a significant change of the instrumental profile, which leads to a notable offset between the pre- and post-upgrade RVs and activity indices. Thus, following Trifonov et al. (2020) we ran SERVAL independently on the post and pre-fiber upgrade data, and we always treated the pre- and post-HARPS-DRS and SERVAL results as taken from two independent instruments.

The HARPS data were obtained between February 2005 and July 2019 with a total temporal baseline of 5257 d. The pre fiber upgrade RVs have a weighted root mean square of $w\text{rms}_{\text{HARPS-pre}} = 8.34 \text{ m s}^{-1}$ and a median RV uncertainty of $\hat{\sigma}_{\text{HARPS-pre}} = 1.04 \text{ m s}^{-1}$, whereas the post upgrade data have $w\text{rms}_{\text{HARPS-post}} = 7.83 \text{ m s}^{-1}$ and $\hat{\sigma}_{\text{HARPS-post}} = 0.65 \text{ m s}^{-1}$, respectively.

Since most of our spectra were taken in three consecutive measurements per visit, we decided to average out the RV measurements in nightly-averaged bins in order to compensate for the contribution of short-term, stellar p-mode pulsations (e.g. Dumusque et al. 2011; Chaplin et al. 2019). As a result, for our orbital analysis, we used nine nightly averaged RV measurements taken prior to the fiber upgrade and 32 nightly averaged measurements taken after the fiber upgrade.

The nightly-averaged RVs of the pre-upgrade HARPS data have a weighted root mean square (wrms) residual of $w\text{rms}_{\text{HARPS-pre}} = 8.3 \text{ m s}^{-1}$ and a median RV uncertainty of $\hat{\sigma}_{\text{HARPS-pre}} = 1.0 \text{ m s}^{-1}$, whereas the post-upgrade HARPS data have $w\text{rms}_{\text{HARPS-post}} = 7.74 \text{ m s}^{-1}$ and $\hat{\sigma}_{\text{HARPS-post}} = 0.66 \text{ m s}^{-1}$, respectively. The HARPS-SERVAL Doppler measurements, activity index data, and their individual formal uncertainties are available in Table A1 and Table A2.

3.3. CARMENES data

We obtained 12 high signal-to-noise spectra of HD 107148 with the CARMENES⁴ instrument (Quirrenbach et al. 2016; Reiners et al. 2018), mounted on the 3.5 m telescope in Calar Alto, Spain. These spectra were acquired on 15 January 2017, 1 March 2017, and 11 April 2017. We derived precise CARMENES optical

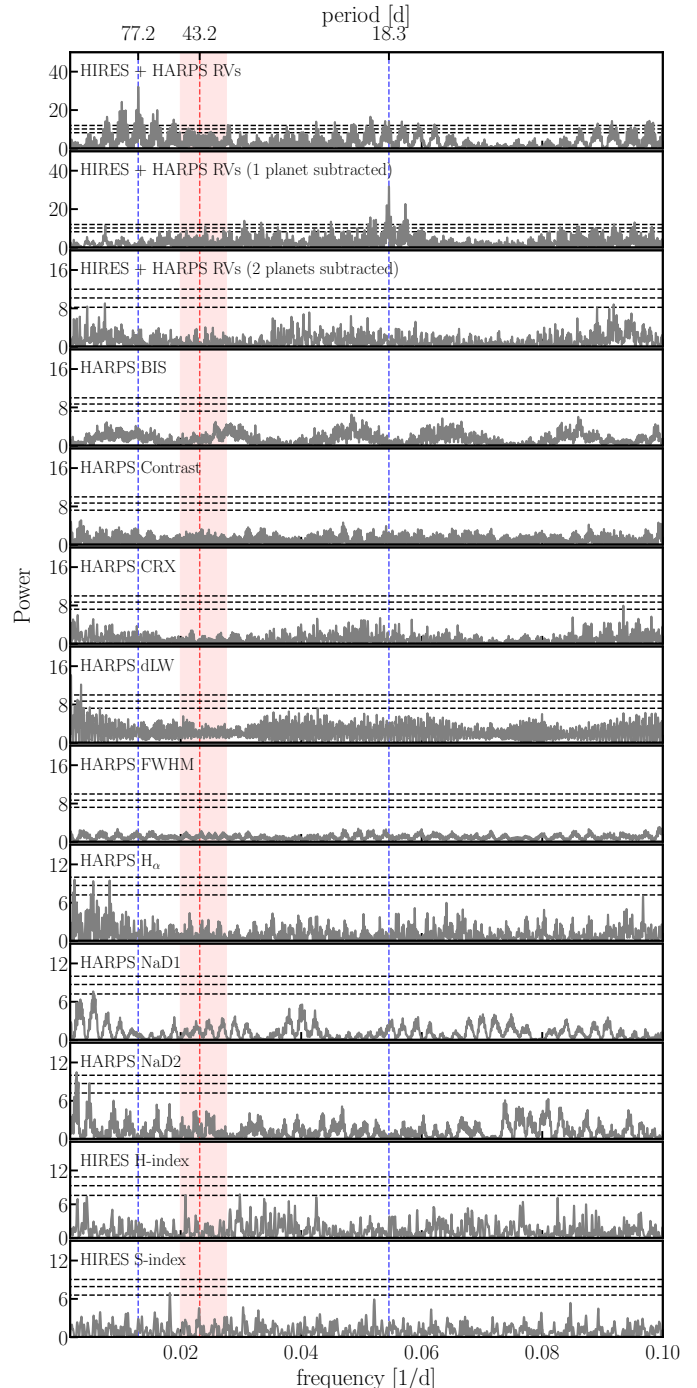


Figure 1. GLS power spectrum for RV data obtained from Keck HIRES and HARPS, as well as stellar activity data obtained from HIRES and HARPS. Horizontal dashed lines indicate FAP levels of 10%, 1%, and 0.1%. Blue vertical dashed lines show the periods of the two significant signals. An upper limit for the most likely rotational period of HD 107148 is indicated with a red vertical dashed line, whereas the $1-\sigma$ uncertainty frequencies of the stellar rotation are shown with a red-transparent region.

⁴ CARMENES stands for; Calar Alto high-Resolution search for M dwarfs with Exo-earths with Near-infrared and optical Echelle Spectrographs. See, <https://carmenes.caha.es/>

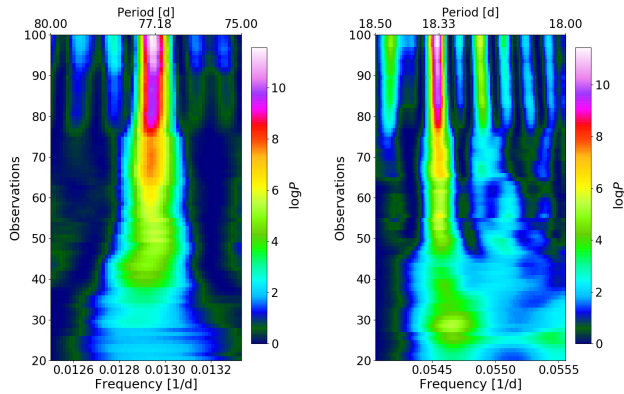


Figure 2. Stacked-Bayesian GLS periodogram of the RV data of HD 107148 focused at the 77 d signal (left), and on the signal at 18 d (right). The s-BGLS of the 77 d signal is calculated by fitting for the RV offset between HIRES, HARPS-pre, and HARPS-post. Similarly, the s-BGLS of the 18 d signal was calculated on the RV residuals of a fit where the signal at 77 d has been removed.

and near-IR RV measurements and activity indicators using the SERVAL pipeline, in the same way we did for HARPS (see Sect. 3.2).

The nightly averaged data resulted in only three precise CARMENES RV measurements in the optical and three in the near-IR, respectively. We find that the small number of CARMENES RVs is insufficient for a significant contribution to our orbital solution, thus, these were not used in combination with HARPS and HIRES. Nonetheless, we investigated the consistency of the CARMENES data with respect to the orbital solution derived with the HIRES and the HARPS RV data sets (see Sect. 4.2). The individual CARMENES Doppler measurements, activity indices, and their individual formal uncertainties are available in Table A3 and Table A4.

4. ANALYSIS AND RESULTS

4.1. Periodogram analysis

We inspected the available RV and activity indicator data for significant periodicity using the generalized Lomb-Scargle periodogram (GLS; Zechmeister & Kürster 2009). As our significance threshold, we adopted the analytically calculated false-alarm probability (FAP) level of $<0.1\%$ as defined in Zechmeister & Kürster (2009). Fig. 1 shows the resulting GLS periodograms for the radial velocities and the stellar activity time series. The ordinate axis indicates the ZK GLS power (Zechmeister & Kürster 2009), the abscissa indicates the scanned frequency, while horizontal dashed lines indicate FAP levels of 10%, 1%, and 0.1% from bottom to top. The first three panels show the GLS pe-

riodograms of the combined HARPS + HIRES RVs after their mutual RV offset and significant signals were subtracted. This being said, the first three panels represent residual GLS periodograms of; a flat-model (i.e., only RV offsets modeled), one-planet fit, and a two-planet fit, respectively. The two top GLS periodograms show two significant signals, indicated in all panels with vertical blue-dashed lines. The flat-model residuals of the HIRES and HARPS data indicate a significant period of 77.2 d, which is consistent with that reported in Butler et al. (2017). We are, however, unable to recover the 48 d period originally reported by Butler et al. (2006). We conclude that the literature period of $P_b \sim 48$ d for HD 107148 b is an aliasing artifact of the new (true) 77.2 d planetary signal and the ~ 29 d period of the lunar cycle, which must have affected the HIRES observation schedule. Evidence for that is the strong 29.6 d peak in the HIRES window function shown in Fig. A1. Indeed, $P_{\text{alias}} = 1/(f_{\text{WF}} - f_{\text{pl.}}) = 1/(\frac{1}{29.6\text{d}} - \frac{1}{77.2\text{d}}) = 48$ d.

After a Keplerian model fits the 77.2 d signal, its residuals show a second significant period around ~ 18.3 d, which we interpret as evidence of a possible second planetary companion in the HD 107148 system. We find that the 18.3 d signal becomes evident thanks to the additional HARPS RVs. After performing a simultaneous two-planet Keplerian fit using these periods as an initial guess, no significant power remains in the residuals.

In Fig. 1 the most probable stellar rotational period and its $1-\sigma$ range of frequencies are indicated with a red vertical dashed line and red-region. These were calculated as $P_{\text{rot}}/\sin i = 2\pi R_*/v \sin i$. Using the radius and projected rotational velocity from Table 1, we derived an upper limit for the stellar rotation period $P_{\text{rot}} = 43.2 \pm 6.9$ d, which as Fig. 1 indicates is sufficiently far in frequency space from any of the planetary signals. Nevertheless, the estimated rotational period of the star only represents an upper limit for the actual rotational period due to the unknown inclination of the system. At this point of the GLS analysis, we assumed that there is still a possibility that the significant ~ 18 d signal could be induced by stellar activity. Therefore, as a mandatory sanity check, we inspected the HIRES and HARPS stellar activity indicators to check for possible effects caused by the star itself that could explain the 18 d and the 77 d signals.

The remaining periodograms in Fig. 1 show the HIRES and HARPS stellar activity indicators as labeled in the panels. There are no significant periods in the stellar activity data that coincide with the planetary orbital frequencies. However, it is worth noting that there are peaks in the HARPS' dLW, H α , and NaD2 that can

Table 2. Best-fit parameters obtained from a Simplex MLE optimization and errors determined from an MCMC analysis, assuming a coplanar edge-on configuration.

Parameter	Planet c	Planet b
K [m s ⁻¹]	$5.28^{+0.32}_{-0.45}$	$8.75^{+0.38}_{-0.41}$
P [day]	$18.3270^{+0.0008}_{-0.0016}$	$77.185^{+0.01}_{-0.025}$
e	$0.40^{+0.04}_{-0.08}$	$0.15^{+0.02}_{-0.06}$
ω [deg]	308^{+14}_{-10}	223^{+19}_{-16}
M_0 [deg]	60^{+5}_{-16}	318^{+14}_{-24}
a [au]	$0.1415^{+0.0015}_{-0.0015}$	$0.3692^{+0.0037}_{-0.0038}$
$m \sin i$ [M_{jup}]	$0.068^{+0.004}_{-0.005}$	$0.196^{+0.009}_{-0.009}$
$RV_{\text{off, HIRES}}$ [m s ⁻¹]	$1.86^{+0.63}_{-0.37}$	
$RV_{\text{off, HARPS(pre)}}$ [m s ⁻¹]	$-9.97^{+0.36}_{-0.65}$	
$RV_{\text{off, HARPS(post)}}$ [m s ⁻¹]	$0.89^{+0.28}_{-0.37}$	
$RV_{\text{jit, HIRES}}$ [m s ⁻¹]	$3.28^{+0.54}_{-0.27}$	
$RV_{\text{jit, HARPS(pre)}}$ [m s ⁻¹]	$0.00^{+1.78}_{-0.31}$	
$RV_{\text{jit, HARPS(post)}}$ [m s ⁻¹]	$1.17^{+0.53}_{-0.01}$	
χ^2	98.67	
χ^2_{ν}	1.17	
rms [m s ⁻¹]	2.91	
$wrms$ [m s ⁻¹]	2.45	
$-\ln \mathcal{L}$	-224.98	
$N_{\text{RV data}}$	100	
Epoch	2451553.08	

be considered significant at low frequencies, which could mean that HD 107148 is a somewhat weakly active star.

As an additional test to our GLS analysis of the available activity indicators, we investigated the coherence of the two significant RV signals around 18 d and 77 d, by performing a stacked-Bayesian GLS periodogram test (s-BGLS; [Mortier et al. 2015](#); [Mortier & Collier Cameron 2017](#)) of the RV data. [Fig. 2](#) shows the results from the s-BGLS analysis. To construct the s-BGLS periodograms, we applied the normalization as in [Mortier & Collier Cameron \(2017\)](#) and fitted for the mutual RV offsets between the HIRES, the HARPS-pre, and the HARPS-post data. Both signals show growth of their signals probability over the complete time-span of the observations, which is a strong indication for their planetary origin. Therefore, we conclude that the 77 d and 18 d signals are of planetary nature, and we further base our Keplerian analysis on adopting the two-planet hypothesis for HD 107148.

4.2. Orbital analysis

To model the planetary orbits from the available precise Doppler data of HD 107148, we used the **Exo-Striker**⁵ ([Trifonov 2019](#)) exoplanet toolbox. We used a Nelder-Mead (Simplex) algorithm ([Nelder & Mead 1965](#)), which optimizes the likelihood ($-\ln \mathcal{L}$) value of the adopted RV model. This is a classical maximum Likelihood Estimator (MLE) scheme, which converges to the maximum $-\ln \mathcal{L}$ value, returning the "best-fit" Keplerian orbital parameters. The **Exo-Striker** offers two Keplerian modeling schemes; a pure unperturbed multi-Keplerian model, and a more complex N-body algorithm, which models the RVs by calculating the mutual gravitational perturbations between the massive bodies in the system (see, e.g., [Tan et al. 2013](#); [Trifonov et al. 2014, 2019](#)). The latter model seems appropriate in the context of the warm-pair of relatively massive planets evident in the HD 107148 data, where dynamics cannot be neglected. However, for accurate orbit calculation, the N-body model requires a sufficiently small integration time-step of at least $P_{\text{inner planet}}/100$, or $dt_{\text{N-body}} \sim 0.18$ d, which, over the temporal baseline of the RV data of ~ 20 yr, makes this model computationally too expensive. It is worth noting that we performed a quality test of a two-planet Keplerian MLE and alternative N-body MLE best-fits. We did not find a significant difference in their $\ln \mathcal{L}$, meaning that the RV data does not have the needed quality to constrain the dynamical properties of the system, or the secular dynamical time scales of the system are much longer than the temporal baseline of the HIRES and HARPS data (see details in [Sect. 4.4](#)). Thus, we find that the pure multi-Keplerian model is entirely sufficient to precisely describe the orbital configuration of HD 107148, given the available RV data, and it was adopted in this work.

Nonetheless, for testing coplanar inclined orbital geometries, we naturally applied an N-body model MLE fitting. Mutually inclined configurations are very ambiguous and cannot be effectively constrained given the available RV data, and are thus not considered in our analysis.

In our adopted MLE scheme, we fitted for the zero point RV offsets of the HIRES, the HARPS-pre, and the HARPS-post data, and the spectroscopic Keplerian parameters of each planet included in the modeling, namely the RV semi-amplitude K , the orbital period P , the eccentricity e , the argument of periastron ω and the mean anomaly M_0 . Since we adopted a pure Keplerian two-planet model, the planetary inclinations

⁵ <https://github.com/3fon3fonov/exostriker>

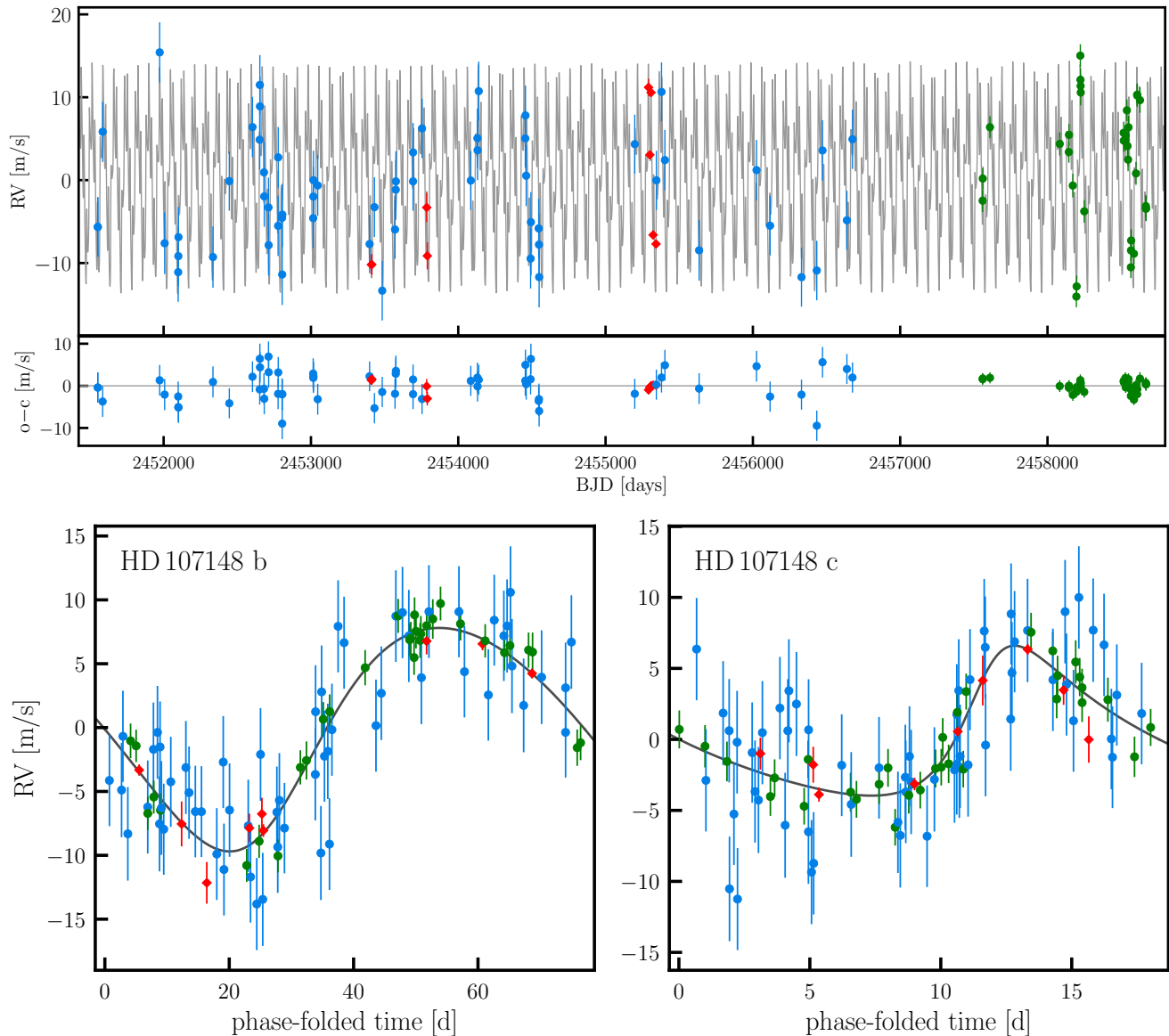


Figure 3. *Top panel:* Doppler radial velocity measurements of HD 107148 from HIRES (blue) and HARPS (red and green, pre and post fiber correction, respectively) modeled with a two-planet Keplerian model (black curve) along with the corresponding residuals beneath. *Bottom panels:* Phase-folded planetary signals fitted to the data, after the respective other planetary signal is subtracted. Left: HD 107148 b, right: HD 107148 c. The data uncertainties include the estimated RV jitter.

i and the difference of the orbital ascending node $\Delta\Omega$ cannot be accessed even if the RV data is sensitive to these parameters⁶. Therefore, we assumed only a coplanar and edge-on configuration of the HD 107148 system (i.e., $i=90^\circ$ and mutual orbital inclination $\Delta i=0^\circ$). Following Baluev (2009), we also fitted for the white-noise variance of each RV data set. We added the RV "jitter" term in quadrature to the nominal RV uncertainties, and

it also presents a penalty-term in our model's likelihood (see Baluev 2009, for the functional form of the $\ln \mathcal{L}$).

We evaluated the posterior probability distribution of the fitted parameters, by adopting the affine-invariant ensemble Markov chain Monte Carlo (MCMC) sampler (Goodman & Weare 2010) using the `emcee` package (Foreman-Mackey et al. 2013), which is integrated within the `Exo-Striker` tool. We explored the parameter space by adopting non-informative flat priors, the range of which we estimated experimentally during the course of our MLE minimization analysis. Since we were more interested in studying possible parameter correla-

⁶ In rare cases of strongly interacting planetary systems, an N-body model can constrain the orbital alignment. See, e.g., the case of the GJ 876 system (Rivera et al. 2010; Nelson et al. 2016)

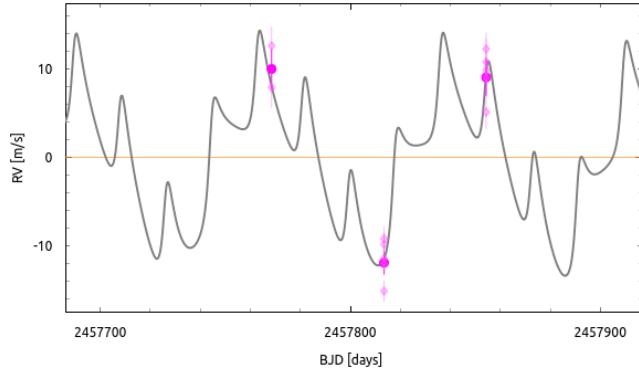


Figure 4. Radial velocity measurements of HD 107148 from CARMENES fitted with a variable RV offset to the best-fit, two-planet Keplerian model constructed from the HARPS and HIRES RV data (see Fig. 3). The individual consecutive measurements are shown with transparent magenta diamonds, whereas the nightly averaged RV measurements are shown with filled magenta circles.

tions and estimating the parameter uncertainties from the posterior distribution, we ran the MCMC chains starting from the "best-fit" parameters returned by the MLE optimization scheme. In our MCMC scheme, we used a setup of 200 walkers, 1 000 burn-in samples, which we discarded from the analysis, followed by 5 000 MCMC samples from which we constructed the parameter posterior distribution. We evaluated the sampler acceptance fraction, which should be between 0.2 and 0.5, to consider the MCMC chains converged (see Foreman-Mackey et al. 2013). The $1\text{-}\sigma$ parameter uncertainties in this work were chosen as the 68.3% confidence levels of the posterior parameter distribution.

We have also tested the sensitivity of our obtained results due to possible correlated RV noise by applying a quasi-periodic Gaussian processes kernel together with a Bayesian nested sampling following an approach as in Stock et al. (2020). We found no significant differences to our obtained results based on our MLE+MCMC scheme that does not incorporate an additional correlated noise model in the form of a Gaussian process. Hence, the omission of a correlated noise model can be justified in the case of HD 107148. In particular, its inclusion has also not been favored significantly by the Bayesian log-evidence.

4.3. Model comparison results

As a means to firmly constrain the orbital configuration of the system, we prepared different competing MLE model schemes with different degrees of freedom (and number of planets), and inspected the quality of their "best-fits". We performed two quality tests: (i) we compared the difference of the MLE fit's likeli-

hood as $\Delta \ln \mathcal{L} = |\ln \mathcal{L}_{\text{complex model}}| - |\ln \mathcal{L}_{\text{simpler model}}|$, (ii) we calculated and compared their Bayesian information criterion (BIC) values. The BIC is defined as $\text{BIC} = k \ln(n) - 2 \ln(\mathcal{L})$, with the number of free parameters k , the number of measurements n and the model's likelihood \mathcal{L} . Widely accepted values for a strong statistic evidence when comparing two models are $\Delta \ln \mathcal{L} > 7$ ⁷ and $\Delta \text{BIC} > 10$ (Kass & Raftery 1995). Thus we adopted these thresholds to claim a significant model improvement. The results of this evaluation can be found in Table 3.

First, we constructed our null model, for which free parameters are the RV offsets and jitters and which contains no planets (model "0"). Then, we injected a combination of Keplerian signals given the information from our GLS test (Sect. 4.1). Alternative models "1" and "2" were constructed assuming only one planet with a period of ~ 77 d (HD 107148 b), whose orbital shape was set to be either strictly circular or allowed to be eccentric. In the circular model "1", the planet's eccentricity was forced to $e = 0$ and its argument of periastron ω was undefined, while for the eccentric model "2", both e and ω , were kept as free fit parameters. Analogously, the following models "3" to "6" were constructed as the possible combinations of two planets with periods of ~ 77 d (HD 107148 b) and ~ 18 d (HD 107148 c) whose orbits were either strictly circular or allowed to be eccentric.

A comparison between models "2" and "6" shows that assuming a second planet greatly improves the fit, with the likelihood improving by $\Delta \ln \mathcal{L} = 62.37$ and the BIC improving by $\Delta \text{BIC} = 101.71$. While there is a significant improvement for model "6" against models "3" and "4" according to our adopted thresholds, there is only weak evidence for model "6" against model "5" with $\Delta \ln \mathcal{L} = 7.16$ and $\Delta \text{BIC} = 5.11$. Unlike the likelihood, which shows a significant improvement, the BIC takes the numbers of parameters into account, thus providing a more meaningful way of comparing the models. However, despite ΔBIC not being sufficiently large enough to claim a significant improvement, we chose model "6" for the final orbital solution of this work and our further analysis, as it still maximizes both $\Delta \ln \mathcal{L}$ and ΔBIC with respect to our null model.

Table 2 lists the best-fit parameters for our adopted model "6" with error estimates obtained from an MCMC as described in Sect. 4.2. The posterior results of the MCMC analysis for our adopted model are shown in

⁷ A relative probability of $R = e^{\Delta \ln \mathcal{L}}$ corresponds to $\sim 0.1\%$ FAP for $\Delta \ln \mathcal{L} = 7$, which is necessary for a significant detection (see Anglada-Escudé et al. 2016)

Table 3. Comparison between the quality of the fits for different models. Circular orbit means $e = 0$, ω undefined and eccentric orbit means that e and ω were kept as fit parameters.

Number	Model	$\ln \mathcal{L}$	BIC	$\Delta \ln \mathcal{L}$	ΔBIC
0	No planet	-337.89	689.60
1	Only planet b (circular orbit)	-289.35	606.33	48.54	83.27
2	Only planet b (eccentric orbit)	-287.35	611.53	50.54	78.07
3	Two planets (both circular orbits)	-245.31	532.07	92.58	157.53
4	Two planets (only planet b eccentric orbit)	-243.14	536.94	94.75	152.66
5	Two planets (only planet c eccentric orbit)	-232.14	514.93	105.75	174.67
6	Two planets (both eccentric orbits)	-224.98	509.82	112.91	179.78

Fig. A3. From these, we could derive the planetary periods $P_b = 77.185^{+0.01}_{-0.025}$ d, $P_c = 18.3270^{+0.0008}_{-0.0016}$ eccentricities $e_b = 0.40^{+0.04}_{-0.08}$, $e_c = 0.15^{+0.02}_{-0.06}$, and masses $m_b \sin i = 0.196^{+0.009}_{-0.009} M_{\text{jup}}$, $m_c \sin i = 0.068^{+0.004}_{-0.005} M_{\text{jup}}$. Model "6" is further illustrated in the top panel of Fig. 3, where the RV time series of both HARPS and HIRES data are shown together with the RV residuals on the bottom. The bottom two panels of Fig. 3 show the individual planetary signals, where the RVs were phase-folded with the best-fit orbital periods (HD 107148 b on the left and HD 107148 c on the right) after subtracting the other planet's signal.

Fig. 4 shows our CARMENES visual channel data (VIS) over-plotted on the best-fit model "6" from the HARPS and HIRES data. As we mentioned in Sect. 3.3, the CARMENES data are very sparse and taken only at three effective epochs. We find that their effective weight to the orbital solution is low, and thus they were not included in the orbital analysis. Nonetheless, we show the consistency of the CARMENES-VIS data to model "6" by fitting an RV offset and jitter, while all other parameters in model "6" were kept fixed. The CARMENES near-IR data we obtain are showing much lower precision and were thus not tested. From Fig. 4 the high precision of the CARMENES data can be assessed, which is in excellent agreement with our adopted model constructed by fitting the HIRES and the HARPS RVs. The nominal 11 CARMENES-VIS channel RVs have a median uncertainty of 1.79 m s^{-1} , and a weighted rms around the best-fit of $wrms = 2.41 \text{ m s}^{-1}$, whereas the three nightly averaged epochs have an RV weighted rms of $wrms = 1.07 \text{ m s}^{-1}$, which is of the same order of precision as HARPS, and better than HIRES (see also Trifonov et al. 2018; Kaminski et al. 2018, for similar conclusions). We note, however, that these estimates in the context of HD 107148, are coming from low-number statistics. While the CARMENES data were not used in our orbital analysis, these RVs further strengthen our two-planet hypothesis of the HD 107148 system due

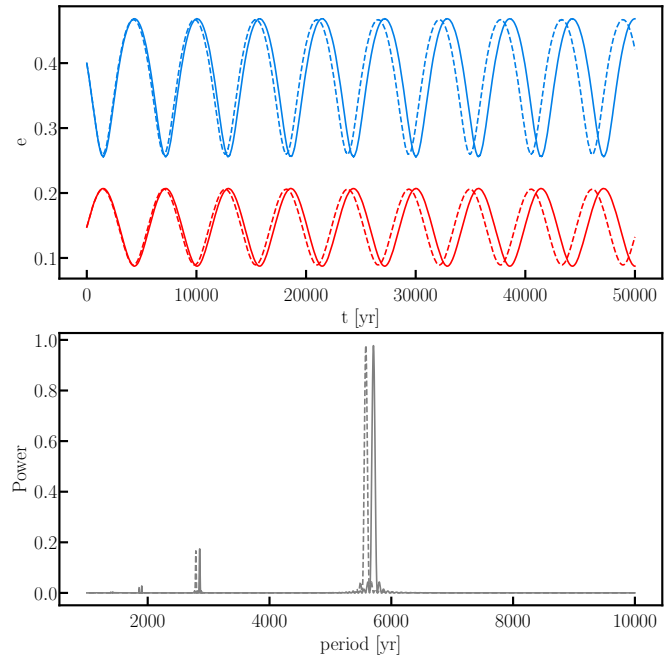


Figure 5. Eccentricity evolution of HD 107148 b (red) and HD 107148 c (blue) using an MVS algorithm with (dashed lines) and without (solid lines) general relativistic corrections. *Top panel:* Evolution of the eccentricities. *Bottom panel:* GLS periodograms of the eccentricity values, peaking at $P = 5707.52$ yr (MVS, solid line) and $P = 5581.36$ yr (MVS-GR, dashed line). The smaller, shorter period GLS peaks are high-frequency harmonics of the true periods.

to their strong agreement with our two-planet, best-fit model and its uncertainties.

4.4. Dynamical analysis

The HD 107148 b & c planets orbit their star in close proximity and are consistent with significant eccentricities. Therefore, we find it essential to study the system's long-term stability and dynamical characteristics. For our dynamical analysis, we adopted a numerical scheme similar to that used by Trifonov et al. (2020) for the eccentric two-planet system GJ 1148. We performed N-body simulations of the orbital evolution of our adopted

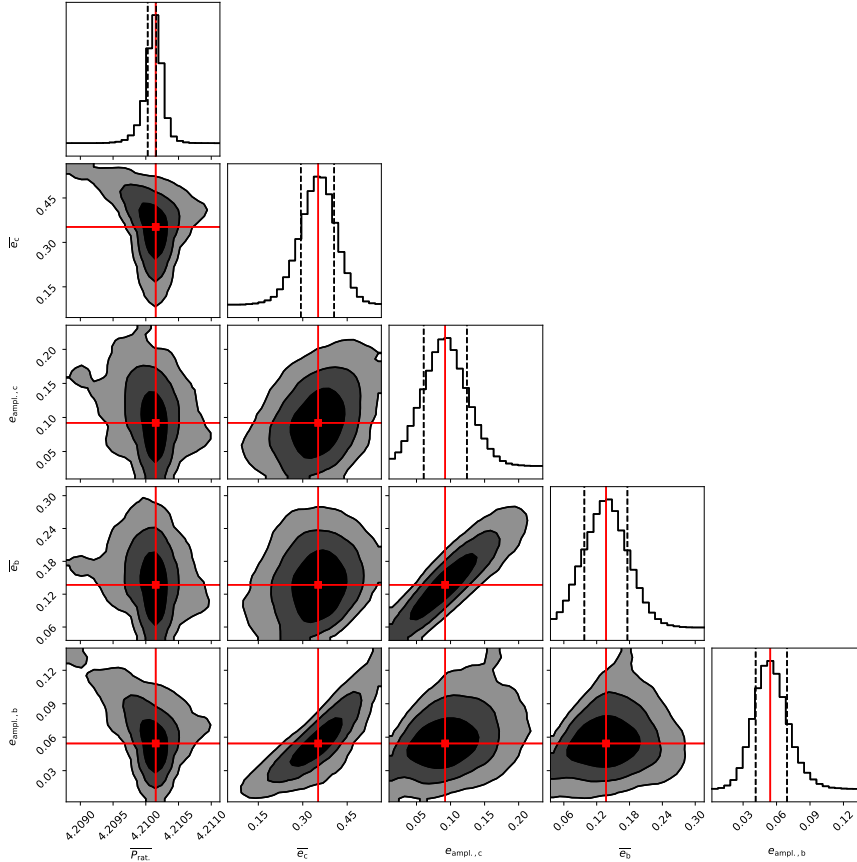


Figure 6. Distribution of the dynamical properties of the MCMC posteriors integrated for 10 Myr. The two-dimensional contours indicate 1-, 2- and 3- σ confidence intervals of the derived posterior distribution. The red crosses indicate the median of the posterior probability distribution. Top to bottom, and left to right: Mean orbital period ratio of the planets P_{rat} , mean planetary eccentricities and eccentricity amplitudes $\langle e_c \rangle$, $e_{\text{ampl.,c}}$, $\langle e_b \rangle$ and $e_{\text{ampl.,b}}$, respectively.

best-fit (Model "6") and the achieved MCMC posterior parameter distribution of this model.

We integrated orbits for 10 Myr using the Wisdom-Holman N-body integrator included in the **Exo-Striker** (also known as MVS, [Wisdom & Holman 1991](#)), and a flavor of the Wisdom-Holman integrator, which can calculate the General Relativistic precession effects (MVS-GR, see, [Trifonov et al. 2020](#)). With the latter integrator, we aimed for a more realistic picture of the long-term evolution of the HD 107148 system, keeping in mind the moderately close and eccentric orbits of HD 107148 c & b, which are affected by GR precession. We adopted a small numerical time step of 0.2 d, which we find sufficient for the accurate integration of the system. While the system is likely very old (see [Table 1](#)), the 10 Myr integrations cover ~ 200 million orbits of the innermost planet HD 107148 c, which we find adequate for deriving conclusions about the system's long-term stability.

Similarly to [Trifonov et al. \(2020\)](#), we monitored the evolution of the planetary semi-major axes and eccentricities as a function of integration time and rejected orbital configurations as unstable if at any given time a_b or a_c exceeded their starting values by 20%, or if e_b or e_c became too large and led to crossing orbits. Since the HD 107148 b & c planets are eccentric yet well separated at the period ratio above the 4:1 commensurability, we also monitored the evolution of the period ratio of the planets HD 107148 b and c as well as the characteristic resonance angles of the 4:1 MMR configuration;

$$\theta_1 = \lambda_c - 4\lambda_b + 3\varpi_b \quad (1)$$

$$\theta_2 = \lambda_c - 4\lambda_b + \varpi_c + 2\varpi_b \quad (2)$$

$$\theta_3 = \lambda_c - 4\lambda_b + 2\varpi_c + \varpi_b \quad (3)$$

$$\theta_4 = \lambda_c - 4\lambda_b + 3\varpi_c, \quad (4)$$

where $\varpi_{b,c} = \Omega_{b,c} + \omega_{b,c}$ are the planetary longitudes of periastron, $\lambda_{b,c} = M_{0b,c} + \varpi_{b,c}$ are the mean longitudes. Further, we monitored the secular apsidal angle

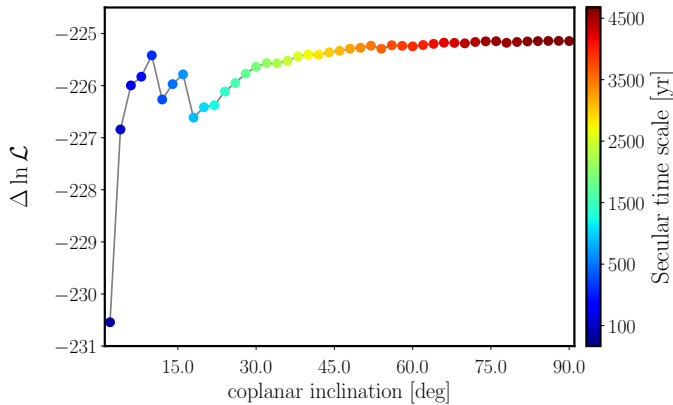


Figure 7. Goodness of coplanar inclined dynamical fits. All fits are long-term stable, color coded is the secular time scales of the orbital osculation (e.g., see, Fig. 5).

$\Delta\omega$, which is defined as:

$$\Delta\omega = \omega_c - \omega_b, \quad (5)$$

which, if librating around a fixed angle, could indicate that the dynamics of the system is dominated by secular interactions.

The integration of the best-fit shows that the HD 107148 system is long-term stable. The semi-major axes stay constant over the 10 Myr of integration time, but we observe a notable osculation of the planetary orbital eccentricities. The top panel of Fig. 5 shows the evolution of the eccentricities of the planets using both MVS (solid lines) and MVS-GR (dashed lines). The eccentricities can be seen osculating around their mean values of $\bar{e}_b = 0.14 \pm 0.04$, $\bar{e}_c = 0.35 \pm 0.06$ with different secular times-scales for the MVS and the MVS-GR runs. The bottom panel of Fig. 5 shows a GLS periodogram of the eccentricity time series, calculated from a 500 000 yr evolution, which indicates an osculation with a period of 5707 d for the MVS and a somewhat shorter period near 5581 d for the MVS-GR. For the best fit, we derived a mean period ratio of $P_{\text{rat.}} = 4.21$ and, θ_1 , θ_2 , θ_3 , θ_4 , $\Delta\omega$, circulating between 0° and 360° . A closer inspection of the trajectory evolution of the resonance angles confirmed that there is no fixed point libration (see Fig. A2). Therefore, we conclude that the best-fit is stable, but not in a 4:1 MMR or involved in secular resonance dynamics. We also conclude that the high-order General Relativistic effects cannot be neglected in the HD 107148 system for secular time scales. However, they do not affect the system’s stability if not included. Therefore, we continued our stability test over the MCMC posterior probability distribution using MVS.

To access the overall dynamical properties of the system, we chose to evaluate 10 000 randomly selected samples from the full MCMC posterior sample (see Fig. A3) and integrated them with the MVS integrator, the same way we did for our best-fit. This way, we constructed posteriors of the dynamical parameters of the system. In addition, we also constructed posterior distributions of the mean eccentricities, semi-major axes and their amplitudes.

All examined samples are stable for 10 Myr, showing similar dynamical behavior as observed in the best-fit N-body test. Thus, we conclude that the HD 107148 system is generally long-term stable. We find all four resonance angles associated with the 4:1 mean-motion resonant commensurability, θ_1 , θ_2 , θ_3 , θ_4 , and the difference of the orbital arguments of periastron (a.k.a. secular apsidal resonance angle) $\Delta\omega = \omega_c - \omega_b$, circulate between 0° and 360° , indicating no mean-motion resonant behaviour, as shown in Fig. A2.

The posterior probability distribution of the dynamically interesting properties of the HD 107148 system is shown in Fig. 6. These are the mean period ratio of the orbital evolution $P_{\text{rat.}}$, mean planetary eccentricities \bar{e}_c , \bar{e}_b , and eccentricity amplitudes $e_{\text{ampl.,c}}$, $e_{\text{ampl.,b}}$, respectively. The distribution of the mean period ratio shows $P_{\text{rat.}} = 4.21_{-0.03}^{+0.02}$. Generally, the system is consistent with moderate mean eccentricity evolution for both planets; $\bar{e}_c = 0.35_{-0.06}^{+0.05}$, and somewhat lower for the more massive outer planet $\bar{e}_b = 0.14_{-0.04}^{+0.04}$. The eccentricity libration amplitudes drawn from the samples are non-negligible with $e_{\text{ampl.,c}} = 0.09_{-0.03}^{+0.03}$ and $e_{\text{ampl.,b}} = 0.05_{-0.01}^{+0.01}$. Fig. 6 also shows a clear correlation between \bar{e}_b and $e_{\text{ampl.,c}}$, and \bar{e}_c and $e_{\text{ampl.,b}}$.

4.5. Constraining the dynamical masses.

In an attempt to constrain the dynamical masses of HD 107148 b and c, we performed N-body modeling adopting different coplanar inclinations. We inspect the range of fixed coplanar inclinations from $i = 90^\circ$ to 2° with a decreasing step of 2° . That is, for each step we fixed; $i_b = i_c$, $\Delta\Omega = 0^\circ$, and $\Delta i = 0^\circ$, exploring from edge-on to nearly face-on geometries. Thus, we keep the system coplanar, but we increase the masses with a factor of $\sim \sin i$, while optimizing the orbital parameters. This test was made consecutively for better convergence, and the best-fit for i was used as an initial guess for the next fit with lower inclination. For each inclined MLE best-fit, we examine the quality, and the long-term stability in the same ways as we did in Sect. 4.4.

Fig. 7 shows the quality of the dynamical fits as a function of the coplanar inclination. The formally best-fit is achieved at edge-on geometry ($i = 90^\circ$), for which we

achieved similar properties to our two-planet Keplerian (model “6”). We find that the quality of the N-body fits in terms of $\Delta \ln \mathcal{L}$ decreases for lower inclination geometries. Generally, however, all fits up to $i = 4^\circ$ are statistically equivalent, whereas the fit with $i = 2^\circ$ seems to suggest a significantly worse solution.

In terms of long-term stability, we find that all fits are stable, even for inclinations as low as $i = 2^\circ$ leading to planetary masses of $m_b = 1.95 M_{\text{Jup}}$ and $m_c = 5.6 M_{\text{Jup}}$. However, even at these large masses, the HD 107148 system could still be ~ 6.5 mutual Hill radii apart, which is above the $\sim 3.5 R_{\text{Hill,m}}$ limit needed for the system to be considered Hill-stable (see, Gladman 1993). A notable dynamical effect of the larger planetary masses is increasing frequency of the dynamical secular time scales of the system, which is shown color-coded in Fig. 7. For $i = 90^\circ$ it is about ~ 5600 yr (see, e.g., Fig. 5), but for the nearly face-on configuration with $i=2^\circ$ it is down to ~ 400 yr. The relatively short orbital osculation for large masses within the temporal baseline of the RVs could explain the bad fit quality at low i . Therefore, we concluded that our N-body modeling could exclude extremely low inclinations, but overall, we could not constrain the planetary dynamical masses from our RV data. Since orbital inclinations near $i = 90^\circ$ are statistically more likely, and our formally best fit is at $i = 90^\circ$, we conclude that HD 107148 is likely on a near coplanar and edge-on configuration.

5. SUMMARY AND DISCUSSION

We present an updated orbital solution for the G-dwarf exoplanet system HD 107148, and report the detection of a second planet in the system, based on the available archival HIRES data and our newly obtained HARPS data. The original publication of Butler et al. (2006) reported an exoplanet with a period of ~ 48 d, which has since been revised by Butler et al. (2017) to ~ 77 d. We find that the literature orbital period of ~ 48 d for HD 107148 is in fact an alias of the ~ 29 d period of the lunar cycle and the true ~ 77 d signal. We were able to independently confirm the 77 d period, as well as to detect an additional ~ 18 d signal, which we also interpret to be of planetary nature. Similar conclusions have been reached independently by Rosenthal et al. (2021), based on an extended HIRES RV data set.

We qualitatively compare different possible orbital configurations for the system, and we reveal the statistically most likely two-planet solution consistent with the available RV data. We conclude that the HD 107148 system consists of a Solar-type star, orbited by two close planets, a Saturn-sized outer planet with an orbital period of ~ 77 d and a Neptune-sized inner planet with an

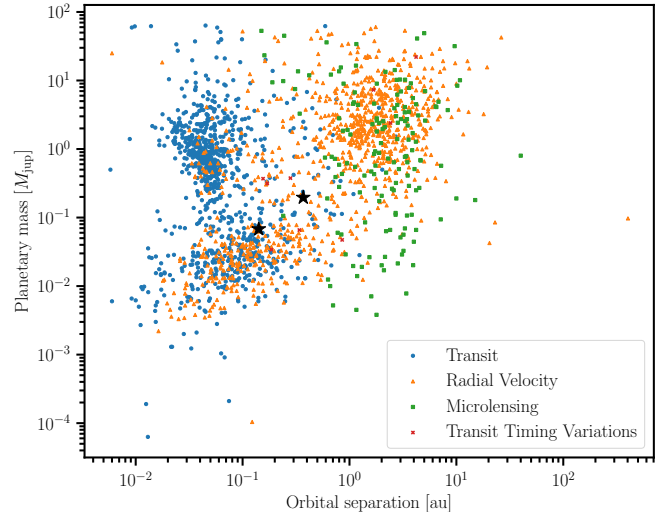


Figure 8. Mass-separation plot for known exoplanets color-coded according to their detection method: *blue circles*: Transit, *orange triangles*: Radial Velocity, *green squares*: Microlensing, *red crosses*: Transit Timing Variations. Due to the generally unknown inclination for planets detected via the Radial Velocity method, their masses should be considered as $m \sin i$. HD 107148 b and c are shown as black stars.

orbital period of ~ 18 d. Fig. 8 shows a mass-separation diagram for known exoplanets⁸. With minimum planetary masses of $m_b \sin i = 0.20 M_{\text{jup}}$, $m_c \sin i = 0.07 M_{\text{jup}}$ and orbital separations of $a_b \sin i = 0.37$ au, $a_c \sin i = 0.14$ au, HD 107148 b falls into an area sparsely populated with planets (upper black star), as it’s less massive than most hot Jupiters and does not orbit as close to its star. HD 107148 c falls onto the massive end of the cluster that includes planets detected using transit methods (lower black star). For a Solar-type star like HD 107148, the two planets are unusually massive and close to their host star. The eccentric configuration of HD 107148 is likely an aftermath of early planet-planet scattering interactions during, or after, the planetary migration epoch. These physical and orbital characteristics of the HD 107148 system make it an ideal target for further research about the formation and evolution of planetary systems.

Further, we provide a dynamical orbital evolution and stability analysis of the HD 107148 system. Our extensive N-body simulations yield that the two-planet system configuration is long-term stable within the entire posterior parameter space, and for a large range of coplanar inclinations. We find that the overall dynamics of the system is not consistent with a resonant behavior, but it exhibits large planetary eccentricity osculations

⁸ <https://exoplanet.eu>, accessed 25 November 2021

with a secular time scale of about 5 500 yr for edge-on configuration, and albeit with much lower confidence, it could be down to 400 yr if the systems' orbit is nearly face-on to the line of sight with Earth. While our fitting results favor a configuration with both planets on eccentric orbits, the evidence is not strong enough to rule out the case of HD 107148 b's orbit being nearly circular at present times. Nevertheless, we find this unlikely since the system is dynamically very active, and the exchange of energy and momentum would periodically trigger eccentricity exchange on secular time scales.

What makes this system particularly interesting is the fact that it also includes a white dwarf companion, orbiting the main-sequence star HD 107148 A with a projected orbital separation of more than 1 000 au. While the WD companion might only have a small gravitational influence on the planetary system, the system is likely to have been covered in a planetary nebula. HD 107148 is one of only a handful known exoplanet systems featuring a WD stellar component. Some of these include the systems; HD 13445 (Gl 86, [Queloz et al. 2000](#); [Els et al. 2001](#); [Lagrange et al. 2006](#)), HD 27442 ([Butler et al. 2001](#); [Chauvin et al. 2006](#); [Mugrauer et al. 2007](#)), HIP 116454 ([Vanderburg et al. 2015](#)), TOI 1259 ([Martin et al. 2021](#)) and HD 147513 ([Mayor et al. 2004](#); [Alexander & Lourens 1969](#)) (for a more detailed list, see [Martin et al. 2021](#)). Assuming that both the WD and the main sequence star have formed at the same time, the age of the system can be constrained from the total age of the WD, which is the sum of its cooling age and the age of its progenitor. However, the age of the HD 107148 system estimated this way is poorly constrained, future observations could help better constraining the mass and cooling age of the white dwarf, allowing for better estimates of the systems age.

Based on observations collected at the European Organization for Astronomical Research in the Southern Hemisphere under ESO programmes: 072.C-0488, 183.C-0972, 097.C-0090, 0100.C-0414, 60.A-9700, 0101.C-0232. Based on observations collected at the Calar Alto (CAHA, Almería, Spain) under program: F17-3.5-019. This research has made use of the SIMBAD database, operated at CDS, Strasbourg, France. This work has made use of data from the European Space Agency (ESA) mission *Gaia* (<https://www.cosmos.esa.int/gaia>), processed by the *Gaia* Data Processing and Analysis Consortium (DPAC, <https://www.cosmos.esa.int/web/gaia/dpac/consortium>). Funding for the DPAC has been provided by national institutions, in particular the institutions participating in the *Gaia* Multilateral Agreement. T.T. and M. K. acknowledge support by the DFG Research Unit FOR

2544 "Blue Planets around Red Stars" project No. KU 3625/2-1. Th. H. acknowledges support by the DFG Research Unit FOR 2544 *Blue Planets around Red Stars*. Th. H. further acknowledges support by the DFG Priority Program SPP 1992 *Exploring the Diversity of Extrasolar Planets*. M.H.L. is supported in part by Hong Kong RGC grant HKU 17305618.

Facilities: ESO-3.6m/HARPS, KECK/HIRES, Calar Alto-3.5m/CARMENES

Software: Exo-Striker ([Trifonov 2019](#)), SERIAL ([Zechmeister et al. 2018](#)),

REFERENCES

- 1997, ESA Special Publication, Vol. 1200, The HIPPARCOS and TYCHO catalogues. Astrometric and photometric star catalogues derived from the ESA HIPPARCOS Space Astrometry Mission
- Alexander, J., & Lourens, J. V. B. 1969, *Monthly Notes of the Astronomical Society of South Africa*, 28, 95
- Anglada-Escudé, G., López-Morales, M., & Chambers, J. E. 2010, *ApJ*, 709, 168, doi: [10.1088/0004-637X/709/1/168](https://doi.org/10.1088/0004-637X/709/1/168)
- Anglada-Escudé, G., Amado, P. J., Barnes, J., et al. 2016, *Nature*, 536, 437
- Bailer-Jones, C. A. L., Rybizki, J., Fouesneau, M., Mantelet, G., & Andrae, R. 2018, *VizieR Online Data Catalog*, I/347
- Baluev, R. V. 2009, *MNRAS*, 393, 969, doi: [10.1111/j.1365-2966.2008.14217.x](https://doi.org/10.1111/j.1365-2966.2008.14217.x)
- Boisvert, J. H., Nelson, B. E., & Steffen, J. H. 2018, *MNRAS*, 480, 2846, doi: [10.1093/mnras/sty2023](https://doi.org/10.1093/mnras/sty2023)
- Butler, R. P., Marcy, G. W., Williams, E., et al. 1996, *PASP*, 108, 500, doi: [10.1086/133755](https://doi.org/10.1086/133755)
- Butler, R. P., Tinney, C. G., Marcy, G. W., et al. 2001, *ApJ*, 555, 410, doi: [10.1086/321467](https://doi.org/10.1086/321467)
- Butler, R. P., Wright, J. T., Marcy, G. W., et al. 2006, *The Astrophysical Journal*, 646, 505, doi: [10.1086/504701](https://doi.org/10.1086/504701)
- Butler, R. P., Vogt, S. S., Laughlin, G., et al. 2017, *AJ*, 153, 208, doi: [10.3847/1538-3881/aa66ca](https://doi.org/10.3847/1538-3881/aa66ca)
- Catalan, S., Isern, J., García-Berro, E., & Ribas, I. 2008, *Monthly Notices of the Royal Astronomical Society*, 387, 1693
- Chaplin, W. J., Cegla, H. M., Watson, C. A., Davies, G. R., & Ball, W. H. 2019, *The Astronomical Journal*, 157, 163
- Chauvin, G., Lagrange, A.-M., Udry, S., et al. 2006, *Astronomy & Astrophysics*, 456, 1165
- Dumusque, X., Udry, S., Lovis, C., Santos, N., & Monteiro, M. 2011, *A140*
- Els, S. G., Sterzik, M. F., Marchis, F., et al. 2001, *A&A*, 370, L1, doi: [10.1051/0004-6361:20010298](https://doi.org/10.1051/0004-6361:20010298)
- Fischer, D. A., Marcy, G. W., & Spronck, J. F. 2013, *The Astrophysical Journal Supplement Series*, 210, 5
- Foreman-Mackey, D., Hogg, D. W., Lang, D., & Goodman, J. 2013, *PASP*, 125, 306, doi: [10.1086/670067](https://doi.org/10.1086/670067)
- Fulton, B. J., Rosenthal, L. J., Hirsch, L. A., et al. 2021, *ApJS*, 255, 14, doi: [10.3847/1538-4365/abfcc1](https://doi.org/10.3847/1538-4365/abfcc1)
- Gaia Collaboration, Prusti, T., de Bruijne, J. H. J., et al. 2016, *A&A*, 595, A1, doi: [10.1051/0004-6361/201629272](https://doi.org/10.1051/0004-6361/201629272)
- Gaia Collaboration, Brown, A. G. A., Vallenari, A., et al. 2018, *A&A*, 616, A1, doi: [10.1051/0004-6361/201833051](https://doi.org/10.1051/0004-6361/201833051)
- Gaia Collaboration, Brown, A. G., Vallenari, A., et al. 2021, *A&A*, 649, A1
- Gladman, B. 1993, *Icarus*, 106, 247
- Goodman, J., & Weare, J. 2010, *Communications in Applied Mathematics and Computational Science*, 5, 65, doi: [10.2140/camcos.2010.5.65](https://doi.org/10.2140/camcos.2010.5.65)
- Howell, S. B., Sobeck, C., Haas, M., et al. 2014, *PASP*, 126, 398, doi: [10.1086/676406](https://doi.org/10.1086/676406)
- Kaminski, A., Trifonov, T., Caballero, J. A., et al. 2018, *A&A*, 618, A115, doi: [10.1051/0004-6361/201833354](https://doi.org/10.1051/0004-6361/201833354)
- Kass, R. E., & Raftery, A. E. 1995, *Journal of the American Statistical Association*, 90, 773
- Kürster, M., Trifonov, T., Reffert, S., Kostogryz, N. M., & Rodler, F. 2015, *A&A*, 577, A103, doi: [10.1051/0004-6361/201525872](https://doi.org/10.1051/0004-6361/201525872)
- Lagrange, A.-M., Beust, H., Udry, S., Chauvin, G., & Mayor, M. 2006, *A&A*, 459, 955
- Lo Curto, G., Pepe, F., Avila, G., et al. 2015, *The Messenger*, 162, 9
- Marcy, G. W., & Butler, R. P. 1992, *PASP*, 104, 270, doi: [10.1086/132989](https://doi.org/10.1086/132989)
- Marcy, G. W., Butler, R. P., Fischer, D., et al. 2001, *ApJ*, 556, 296, doi: [10.1086/321552](https://doi.org/10.1086/321552)
- Martin, D. V., El-Badry, K., Kunovac Hodžić, V., et al. 2021, *arXiv e-prints*, arXiv:2101.02707, <https://arxiv.org/abs/2101.02707>
- Mayor, M., Udry, S., Naef, D., et al. 2004, *Astronomy & Astrophysics*, 415, 391
- Mayor, M., Pepe, F., Queloz, D., et al. 2003, *The Messenger*, 114, 20
- Mortier, A., & Collier Cameron, A. 2017, *A&A*, 601, A110, doi: [10.1051/0004-6361/201630201](https://doi.org/10.1051/0004-6361/201630201)
- Mortier, A., Faria, J. P., Correia, C. M., Santerne, A., & Santos, N. C. 2015, *A&A*, 573, A101, doi: [10.1051/0004-6361/201424908](https://doi.org/10.1051/0004-6361/201424908)
- Mugrauer, M., & Dinçel, B. 2016, *Astronomische Nachrichten*, 337, 627, doi: [10.1002/asna.201512306](https://doi.org/10.1002/asna.201512306)
- Mugrauer, M., Ginski, C., & Seeliger, M. 2014, *MNRAS*, 439, 1063, doi: [10.1093/mnras/stu044](https://doi.org/10.1093/mnras/stu044)
- Mugrauer, M., Neuhäuser, R., & Mazeh, T. 2007, *Astronomy & Astrophysics*, 469, 755
- Nelder, J. A., & Mead, R. 1965, *Computer Journal*, 7, 308
- Nelson, B. E., Robertson, P. M., Payne, M. J., et al. 2016, *MNRAS*, 455, 2484, doi: [10.1093/mnras/stv2367](https://doi.org/10.1093/mnras/stv2367)
- Pecaut, M. J., & Mamajek, E. E. 2013, *ApJS*, 208, 9, doi: [10.1088/0067-0049/208/1/9](https://doi.org/10.1088/0067-0049/208/1/9)
- Queloz, D., Mayor, M., Weber, L., et al. 2000, *A&A*, 354, 99
- Queloz, D., Henry, G. W., Sivan, J. P., et al. 2001, *Astronomy and Astrophysics*, 379, 279, doi: [10.1051/0004-6361:20011308](https://doi.org/10.1051/0004-6361:20011308)

- Quirrenbach, A., Amado, P. J., Caballero, J. A., et al. 2016, in Proc. SPIE, Vol. 9908, Society of Photo-Optical Instrumentation Engineers (SPIE) Conference Series, 990812, doi: [10.1117/12.2231880](https://doi.org/10.1117/12.2231880)
- Reiners, A., Zechmeister, M., Caballero, J. A., et al. 2018, A&A, 612, A49, doi: [10.1051/0004-6361/201732054](https://doi.org/10.1051/0004-6361/201732054)
- Ricker, G. R., Winn, J. N., Vanderspek, R., et al. 2015, Journal of Astronomical Telescopes, Instruments, and Systems, 1, 014003, doi: [10.1117/1.JATIS.1.1.014003](https://doi.org/10.1117/1.JATIS.1.1.014003)
- Rivera, E. J., Laughlin, G., Butler, R. P., et al. 2010, ApJ, 719, 890, doi: [10.1088/0004-637X/719/1/890](https://doi.org/10.1088/0004-637X/719/1/890)
- Rosenthal, L. J., Fulton, B. J., Hirsch, L. A., et al. 2021, ApJS, 255, 8, doi: [10.3847/1538-4365/abe23c](https://doi.org/10.3847/1538-4365/abe23c)
- Soto, M. G., & Jenkins, J. S. 2018, A&A, 615, A76, doi: [10.1051/0004-6361/201731533](https://doi.org/10.1051/0004-6361/201731533)
- Stock, S., Nagel, E., Kemmer, J., et al. 2020, A&A, 643, A112, doi: [10.1051/0004-6361/202038820](https://doi.org/10.1051/0004-6361/202038820)
- Tal-Or, L., Trifonov, T., Zucker, S., Mazeh, T., & Zechmeister, M. 2019, MNRAS, 484, L8, doi: [10.1093/mnrasl/sly227](https://doi.org/10.1093/mnrasl/sly227)
- Tan, X., Payne, M. J., Lee, M. H., et al. 2013, ApJ, 777, 101, doi: [10.1088/0004-637X/777/2/101](https://doi.org/10.1088/0004-637X/777/2/101)
- Tokovinin, A., & Lépine, S. 2012, AJ, 144, 102, doi: [10.1088/0004-6256/144/4/102](https://doi.org/10.1088/0004-6256/144/4/102)
- Trifonov, T. 2019, The Exo-Striker: Transit and radial velocity interactive fitting tool for orbital analysis and N-body simulations. <http://ascl.net/1906.004>
- Trifonov, T., Reffert, S., Tan, X., Lee, M. H., & Quirrenbach, A. 2014, A&A, 568, A64, doi: [10.1051/0004-6361/201322885](https://doi.org/10.1051/0004-6361/201322885)
- Trifonov, T., Tal-Or, L., Zechmeister, M., et al. 2020, A&A, 636, A74, doi: [10.1051/0004-6361/201936686](https://doi.org/10.1051/0004-6361/201936686)
- Trifonov, T., Kürster, M., Zechmeister, M., et al. 2017, A&A, 602, L8, doi: [10.1051/0004-6361/201731044](https://doi.org/10.1051/0004-6361/201731044)
- . 2018, A&A, 609, A117, doi: [10.1051/0004-6361/201731442](https://doi.org/10.1051/0004-6361/201731442)
- Trifonov, T., Stock, S., Henning, T., et al. 2019, AJ, 157, 93, doi: [10.3847/1538-3881/aafa11](https://doi.org/10.3847/1538-3881/aafa11)
- Vanderburg, A., Montet, B. T., Johnson, J. A., et al. 2015, ApJ, 800, 59, doi: [10.1088/0004-637X/800/1/59](https://doi.org/10.1088/0004-637X/800/1/59)
- Vogt, S. S., Allen, S. L., Bigelow, B. C., et al. 1994, in Proc. SPIE, Vol. 2198, Instrumentation in Astronomy VIII, ed. D. L. Crawford & E. R. Craine, 362, doi: [10.1117/12.176725](https://doi.org/10.1117/12.176725)
- Vogt, S. S., Radovan, M., Kibrick, R., et al. 2014, PASP, 126, 359, doi: [10.1086/676120](https://doi.org/10.1086/676120)
- Wisdom, J., & Holman, M. 1991, AJ, 102, 1528, doi: [10.1086/115978](https://doi.org/10.1086/115978)
- Wittenmyer, R. A., Clark, J. T., Zhao, J., et al. 2019, MNRAS, 484, 5859, doi: [10.1093/mnras/stz290](https://doi.org/10.1093/mnras/stz290)
- Wittenmyer, R. A., Wang, S., Horner, J., et al. 2013, ApJS, 208, 2, doi: [10.1088/0067-0049/208/1/2](https://doi.org/10.1088/0067-0049/208/1/2)
- Zechmeister, M., & Kürster, M. 2009, A&A, 496, 577, doi: [10.1051/0004-6361:200811296](https://doi.org/10.1051/0004-6361:200811296)
- Zechmeister, M., Reiners, A., Amado, P. J., et al. 2018, A&A, 609, A12, doi: [10.1051/0004-6361/201731483](https://doi.org/10.1051/0004-6361/201731483)

APPENDIX

In this Appendix, we show additional plots, including the HIRES window function, trajectory plots of the resonance angles and the corner plot for our MCMC analysis, as well as tables containing our HARPS and CARMENES data. [Fig. A1](#) shows the window function of the HIRES data of HD 107148 provided by [Tal-Or et al. \(2019\)](#). [Fig. A2](#) shows the trajectory plots of the evolution of the four resonance angles associated with a 4:1 mean motion resonance. [Fig. A3](#) shows the posterior distribution of our MCMC sample of the combined HARPS and HIRES data of HD 107148. [Table A1](#) and [Table A2](#) show the HARPS radial velocity and activity index measurements for HD 107148, derived with the DRS and Serval pipelines. [Table A3](#) and [Table A4](#) show the CARMENES radial velocity and activity index measurements in the visual and near-infrared range, derived with the Serval pipeline.

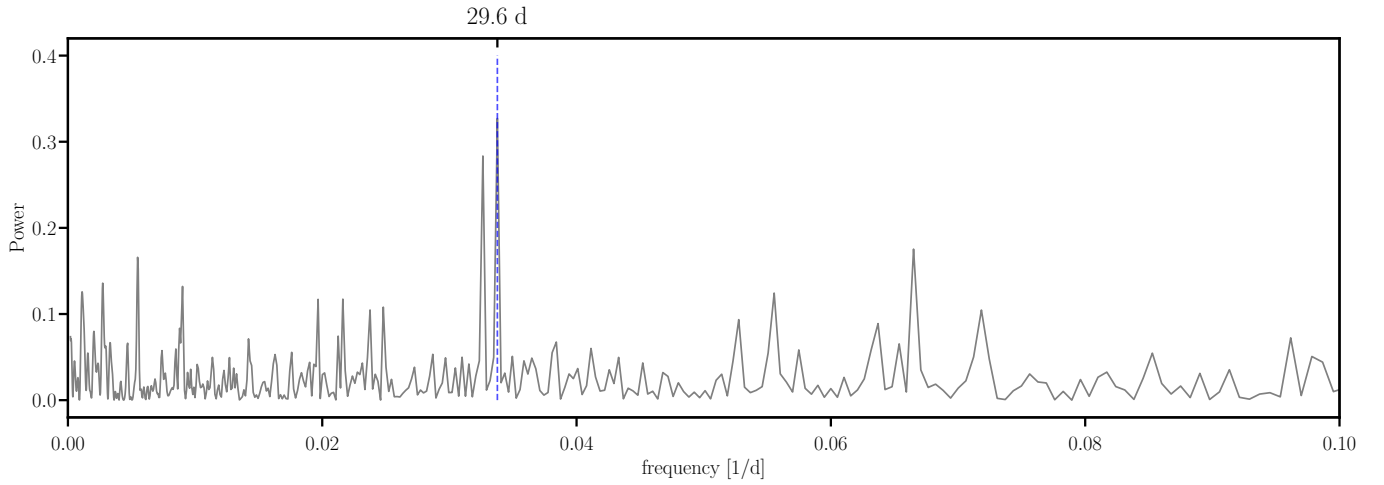


Figure A1. Window function of the HIRES data set. The highest peak at a period of ~ 29.6 d corresponds to the lunar cycle, which affects the Keck-HIRES observational schedule.

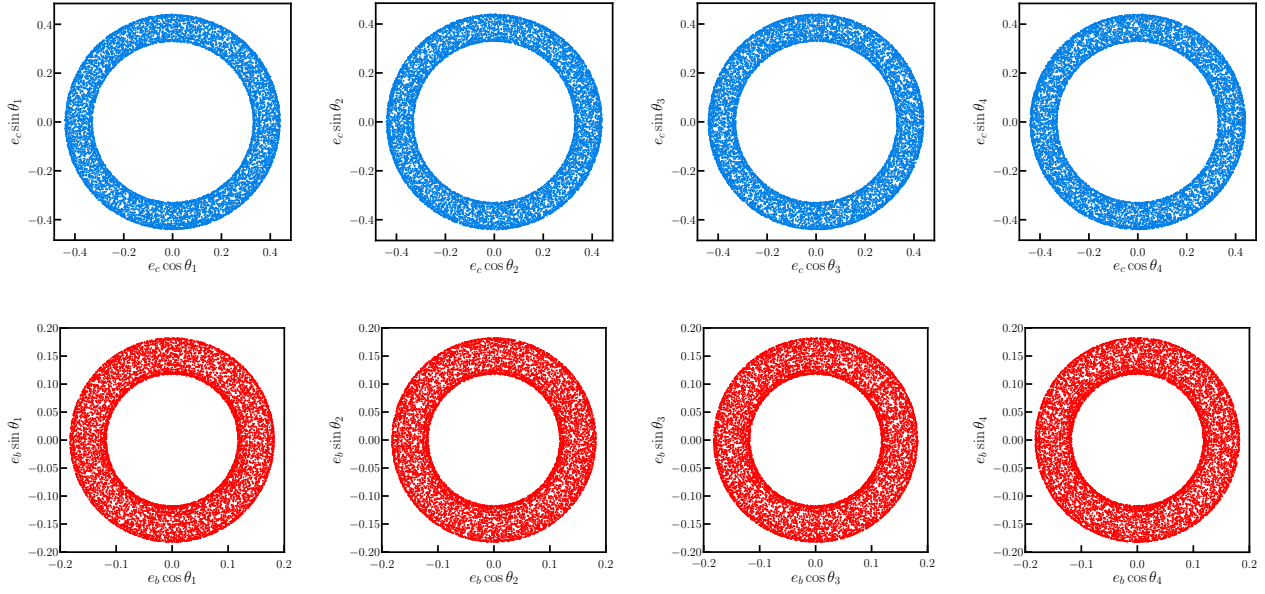


Figure A2. Trajectory plots for the resonance angles θ_1 , θ_2 , θ_3 and θ_4 for HD 107148 b (*red*) and HD 107148 c (*blue*).

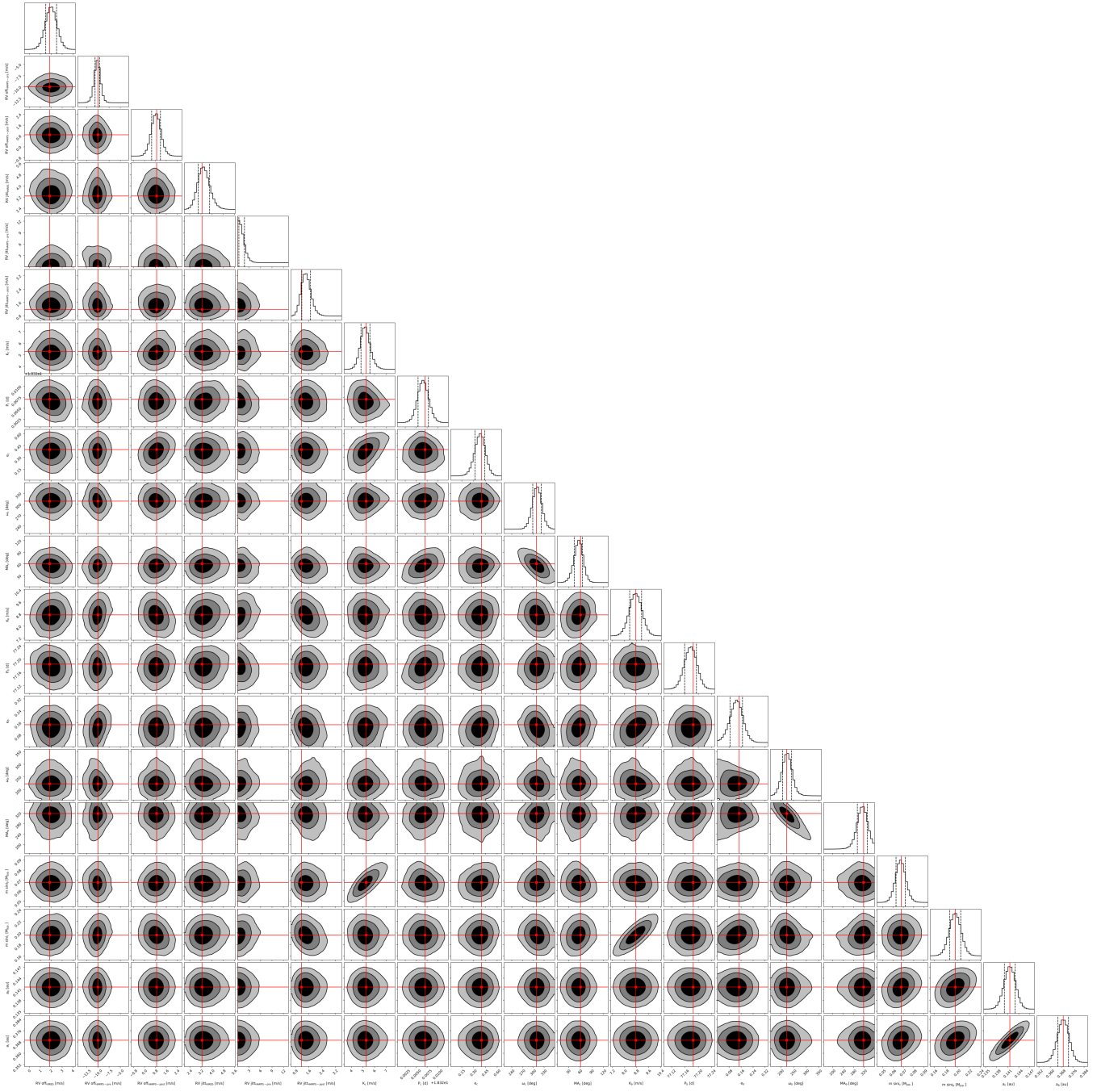


Figure A3. Correlations of the parameter posteriors achieved from the MCMC analysis. Red intersections denote the position of the best-fit values. The two-dimensional contours indicate 1-, 2- and 3- σ confidence intervals of the posterior distribution. *Top to bottom, and left to right:* RV offsets of HIRES and HARPS (pre- and post-fiber upgrade), RV jitters of HIRES and HARPS, K_c , P_c , e_c , ω_c , M_c , K_b , P_b , e_b , ω_b , M_b , $m_c \sin i$, $m_b \sin i$, a_c , a_b .

Table A1. HARPS Doppler measurements and activity index measurements of HD 107148, derived with SERVAL

Epoch [JD]	RV [m s ⁻¹]	σ_{RV} [m s ⁻¹]	CRX [m s ⁻¹]	σ_{CRX} [m s ⁻¹]	dLW [m s ⁻¹ * km s ⁻¹]	σ_{dLW} [m s ⁻¹ * km s ⁻¹]	H α	$\sigma_{H\alpha}$	NaD1	σ_{NaD1}	NaD2	σ_{NaD2}	FWHM [km s ⁻¹]	σ_{FWHM} [km s ⁻¹]	Cont	σ_{Cont}	BIS [km s ⁻¹]	σ_{BIS} [km s ⁻¹]
2453410.74594	-20.18	1.13	7.55	11.25	-52.50	4.15	0.4294	0.0012	0.2858	0.0015	0.3889	0.0020	7.151	0.072	53.21	0.53	-28.54	-0.29
2453412.76455	-20.14	1.26	0.03	11.76	-56.90	4.25	0.4284	0.0013	0.2837	0.0017	0.3858	0.0022	7.156	0.072	53.25	0.53	-27.49	-0.27
2453785.77908	-13.27	1.76	21.94	16.40	-35.70	4.94	0.4318	0.0019	0.2872	0.0025	0.4025	0.0032	7.165	0.072	52.94	0.53	-31.45	-0.31
2453789.82758	-19.10	1.63	3.50	14.15	-36.71	4.62	0.4286	0.0017	0.2876	0.0022	0.3949	0.0028	7.162	0.072	52.99	0.53	-27.70	-0.28
2455291.68074	0.11	1.05	-22.06	11.40	-30.42	4.30	0.4244	0.0011	0.2908	0.0014	0.3823	0.0018	7.158	0.072	52.90	0.53	-24.67	-0.25
2455291.68331	1.88	0.99	11.88	10.46	-29.80	4.55	0.4249	0.0010	0.2908	0.0013	0.3835	0.0017	7.165	0.072	52.88	0.53	-22.14	-0.22
2455291.68564	-0.62	1.08	-8.87	13.25	-26.48	4.25	0.4210	0.0011	0.2926	0.0014	0.3816	0.0019	7.167	0.072	52.88	0.53	-30.23	-0.30
2455291.68824	3.43	1.04	-2.61	11.36	-27.51	4.73	0.4247	0.0011	0.2912	0.0014	0.3828	0.0018	7.163	0.072	52.86	0.53	-24.36	-0.24
2455300.62303	-7.00	0.55	-8.60	7.00	-28.15	4.07	0.4244	0.0006	0.2860	0.0007	0.3873	0.0009	7.164	0.072	52.92	0.53	-28.49	-0.28
2455300.71809	-6.84	0.45	-15.13	6.83	-28.62	3.80	0.4235	0.0005	0.2915	0.0006	0.3763	0.0008	7.167	0.072	52.92	0.53	-29.11	-0.29
2455308.63859	0.60	0.38	-10.61	8.04	-22.02	3.34	0.4230	0.0004	0.2870	0.0005	0.3848	0.0006	7.164	0.072	52.89	0.53	-23.55	-0.24
2455322.64701	-16.58	0.45	-23.44	7.77	-23.96	3.62	0.4245	0.0004	0.2923	0.0006	0.3885	0.0007	7.170	0.072	52.88	0.53	-27.36	-0.27
2455342.62344	-17.67	0.50	-15.81	7.31	-25.33	3.45	0.4260	0.0005	0.2914	0.0006	0.3889	0.0008	7.170	0.072	52.89	0.53	-25.94	-0.26
2457559.61595	-1.92	0.68	-8.10	9.13	2.96	1.62	0.4299	0.0006	0.2905	0.0008	0.3850	0.0010	7.193	0.072	52.67	0.53	-18.78	-0.19
2457559.62209	-1.32	0.69	4.52	8.45	6.29	1.56	0.4315	0.0006	0.2930	0.0008	0.3851	0.0011	7.194	0.072	52.66	0.53	-17.84	-0.18
2457559.62829	-1.52	0.69	1.01	8.58	7.50	1.45	0.4297	0.0006	0.2927	0.0008	0.3846	0.0010	7.194	0.072	52.66	0.53	-16.54	-0.17
2457560.51145	0.64	0.47	11.57	7.05	3.22	0.99	0.4315	0.0005	0.2905	0.0006	0.3787	0.0008	7.195	0.072	52.70	0.53	-15.25	-0.15
2457560.51748	1.13	0.48	12.71	7.05	5.63	1.07	0.4307	0.0005	0.2920	0.0006	0.3806	0.0008	7.194	0.072	52.69	0.53	-16.61	-0.17
2457560.52374	1.52	0.51	8.05	7.45	2.56	1.07	0.4309	0.0005	0.2912	0.0006	0.3787	0.0008	7.194	0.072	52.71	0.53	-15.34	-0.15
2457609.45890	6.20	0.60	8.18	9.26	8.34	1.46	0.4295	0.0006	0.2916	0.0007	0.3812	0.0009	7.192	0.072	52.66	0.53	-15.09	-0.15
2457609.46470	8.48	0.60	6.63	8.66	3.18	1.37	0.4293	0.0006	0.2913	0.0007	0.3807	0.0009	7.188	0.072	52.72	0.53	-16.52	-0.17
2457609.47102	7.16	0.63	8.37	8.89	4.27	1.43	0.4289	0.0006	0.2919	0.0008	0.3793	0.0010	7.193	0.072	52.69	0.53	-15.01	-0.15
2458082.86206	4.21	0.78	-9.27	7.85	7.37	1.78	0.4269	0.0008	0.2924	0.0010	0.3954	0.0013	7.193	0.072	52.69	0.53	-17.15	-0.17
2458082.86809	3.34	0.71	-2.40	7.66	14.87	1.80	0.4276	0.0007	0.3145	0.0009	0.4083	0.0012	7.191	0.072	52.64	0.53	-13.42	-0.13
2458082.87412	8.49	0.79	-21.46	7.16	50.38	3.14	0.4275	0.0008	0.3572	0.0011	0.4405	0.0014	7.189	0.072	52.29	0.52	-17.25	-0.17
2458144.78547	4.92	0.52	2.09	6.35	10.46	1.22	0.4259	0.0005	0.2813	0.0006	0.3865	0.0008	7.189	0.072	52.69	0.53	-15.22	-0.15
2458144.79145	3.98	0.53	-0.15	6.23	6.59	1.38	0.4263	0.0006	0.2804	0.0007	0.3852	0.0009	7.188	0.072	52.70	0.53	-14.17	-0.14
2458144.79767	3.93	0.54	6.28	7.18	7.82	1.24	0.4272	0.0006	0.2798	0.0007	0.3852	0.0009	7.190	0.072	52.71	0.53	-16.48	-0.16
2458145.80913	7.11	0.65	-9.98	7.14	8.02	1.42	0.4256	0.0007	0.2766	0.0008	0.3973	0.0010	7.189	0.072	52.70	0.53	-11.90	-0.12
2458145.81534	6.58	0.63	-12.52	6.56	10.26	1.40	0.4265	0.0006	0.2741	0.0008	0.3954	0.0010	7.189	0.072	52.69	0.53	-16.07	-0.16
2458145.82144	5.38	0.65	-5.41	7.48	9.38	1.42	0.4264	0.0006	0.2761	0.0008	0.3934	0.0010	7.186	0.072	52.70	0.53	-14.57	-0.15
2458171.73165	-0.12	0.78	9.64	11.08	9.11	1.85	0.4285	0.0009	0.2843	0.0009	0.3954	0.0011	7.291	0.073	51.84	0.52	-31.21	-0.31
2458171.73797	0.05	0.82	-3.06	10.94	6.30	2.08	0.4264	0.0009	0.2830	0.0009	0.3949	0.0012	7.296	0.073	51.89	0.52	-32.95	-0.33
2458171.74417	0.81	0.83	5.04	11.41	7.23	1.80	0.4266	0.0009	0.2820	0.0010	0.3937	0.0012	7.285	0.073	51.95	0.52	-26.46	-0.26
2458195.77177	-13.79	0.55	5.68	7.40	7.23	1.38	0.4248	0.0005	0.2837	0.0007	0.3822	0.0009	7.189	0.072	52.69	0.53	-16.87	-0.17
2458195.77803	-12.79	0.54	6.33	7.12	7.06	1.23	0.4253	0.0005	0.2839	0.0007	0.3799	0.0009	7.192	0.072	52.69	0.53	-15.75	-0.16
2458195.78406	-12.88	0.54	6.89	7.76	7.61	1.43	0.4269	0.0005	0.2843	0.0007	0.3825	0.0009	7.192	0.072	52.70	0.53	-18.31	-0.18
2458197.76886	-11.48	0.58	7.76	6.50	7.05	1.29	0.4247	0.0006	0.2854	0.0007	0.3901	0.0009	7.193	0.072	52.69	0.53	-15.85	-0.16
2458197.77518	-12.31	0.57	-2.83	6.89	6.40	1.13	0.4264	0.0006	0.2852	0.0007	0.3894	0.0009	7.192	0.072	52.69	0.53	-17.90	-0.18
2458197.78127	-11.97	0.52	-1.04	7.24	7.44	1.24	0.4255	0.0005	0.2849	0.0006	0.3905	0.0008	7.194	0.072	52.69	0.53	-16.86	-0.17
2458222.76220	18.17	0.70	1.52	7.62	5.31	1.58	0.4286	0.0007	0.2854	0.0009	0.3900	0.0011	7.191	0.072	52.71	0.53	-17.39	-0.17
2458222.76882	15.31	0.77	0.24	9.41	3.66	1.86	0.4281	0.0008	0.2864	0.0010	0.3789	0.0013	7.193	0.072	52.70	0.53	-14.90	-0.15
2458222.77465	14.30	0.66	-6.83	6.58	6.26	1.63	0.4278	0.0006	0.2863	0.0008	0.3803	0.0011	7.194	0.072	52.69	0.53	-13.67	-0.14
2458223.77444	13.00	0.71	-1.28	6.88	5.74	1.58	0.4246	0.0007	0.2877	0.0009	0.3874	0.0012	7.192	0.072	52.70	0.53	-11.55	-0.12
2458223.78055	13.22	0.72	-9.98	7.69	4.24	1.45	0.4243	0.0007	0.2858	0.0009	0.3870	0.0011	7.190	0.072	52.72	0.53	-17.95	-0.18
2458223.78682	12.74	0.87	4.94	9.28	6.03	1.90	0.4237	0.0008	0.2857	0.0011	0.3879	0.0014	7.196	0.072	52.69	0.53	-14.50	-0.15
2458224.70939	10.84	0.78	4.17	8.26	4.19	1.76	0.4296	0.0008	0.2842	0.0011	0.3811	0.0014	7.196	0.072	52.70	0.53	-14.53	-0.15
2458224.71561	12.62	0.59	-4.39	7.02	7.39	1.41	0.4285	0.0006	0.2869	0.0007	0.3794	0.0010	7.192	0.072	52.68	0.53	-14.51	-0.15
2458224.72177	12.92	0.55	-5.42	7.61	8.58	1.11	0.4282	0.0005	0.2839	0.0007	0.3764	0.0009	7.194	0.072	52.68	0.53	-15.94	-0.16
2458225.69613	12.07	0.98	-11.31	8.81	2.48	2.03	0.4232	0.0011	0.2970	0.0014	0.3803	0.0017	7.191	0.072	52.71	0.53	-13.67	-0.14
2458225.70234	9.99	1.06	0.22	10.09	5.05	2.30	0.4200	0.0012	0.2955	0.0015	0.3778	0.0019	7.192	0.072	52.71	0.53	-11.61	-0.12
2458225.70850	12.25	1.02	0.14	9.39	3.27	2.35	0.4209	0.0011	0.2864	0.0014	0.3786	0.0018	7.188	0.072	52.72	0.53	-12.72	-0.13
2458249.46316	-3.42	0.74	3.13	7.03	6.24	1.30	0.4246	0.0008	0.2941	0.0010	0.3796	0.0013	7.193	0.072	52.70	0.53	-16.45	-0.16
2458249.46927	-2.71	0.75	-2.77	7.58	2.76	1.57	0.4234	0.0008	0.2939	0.0010	0.3781	0.0013	7.193	0.072	52.73	0.53	-15.06	-0.15
2458249.47548	-2.56	0.60	-0.06	6.03	3.47	1.29	0.4241	0.0007	0.2847	0.0008	0.3807	0.0011	7.191	0.072	52.71	0.53	-12.57	-0.13
2458516.82380	6.44	0.67	0.23	7.83	3.90	1.57	0.4275	0.0008	0.2841	0.0009	0.4024	0.0012	7.187	0.072	52.73	0.53	-18.82	-0.19

Table A2. HARPS Doppler measurements and activity index measurements of HD 107148, derived with SERVAL (Cont.)

Epoch [JD]	RV [m s ⁻¹]	σ_{RV} [m s ⁻¹]	CRX [m s ⁻¹]	σ_{CRX} [m s ⁻¹]	dLW [m s ⁻¹ * km s ⁻¹]	σ_{dLW} [m s ⁻¹ * km s ⁻¹]	H α	$\sigma_{H\alpha}$	NaD ₁	σ_{NaD_1}	NaD ₂	σ_{NaD_2}	FWHM [km s ⁻¹]	σ_{FWHM} [km s ⁻¹]	Cont	σ_{Cont}	BIS [km s ⁻¹]	σ_{BIS} [km s ⁻¹]
2458516.83563	7.31	0.66	-5.71	8.04	3.34	1.15	0.4277	0.0008	0.2807	0.0009	0.4010	0.0012	7.184	0.072	52.74	0.53	-19.10	-0.19
2458517.85673	6.23	0.62	14.21	6.42	6.51	1.35	0.4282	0.0007	0.2787	0.0009	0.3978	0.0012	7.189	0.072	52.74	0.53	-17.09	-0.17
2458517.86218	5.00	0.70	11.41	6.65	4.17	1.58	0.4290	0.0008	0.2782	0.0009	0.3977	0.0012	7.189	0.072	52.74	0.53	-15.76	-0.16
2458528.86119	5.90	0.61	1.48	7.94	2.10	1.10	0.4286	0.0007	0.2855	0.0008	0.3927	0.0011	7.186	0.072	52.75	0.53	-15.43	-0.15
2458528.86740	5.70	0.65	5.32	9.44	3.80	1.56	0.4289	0.0007	0.2854	0.0009	0.3928	0.0011	7.186	0.072	52.75	0.53	-15.47	-0.15
2458528.87373	5.65	0.64	11.84	8.32	2.27	1.28	0.4283	0.0007	0.2861	0.0009	0.3932	0.0011	7.189	0.072	52.73	0.53	-16.75	-0.17
2458530.89322	6.91	0.52	-9.43	5.50	2.14	1.10	0.4281	0.0005	0.2849	0.0007	0.3953	0.0009	7.183	0.072	52.76	0.53	-18.91	-0.19
2458530.89942	6.64	0.53	1.52	6.29	2.97	1.26	0.4283	0.0005	0.2842	0.0007	0.3962	0.0009	7.189	0.072	52.74	0.53	-17.48	-0.17
2458530.90556	5.29	0.55	0.66	7.16	5.03	1.18	0.4285	0.0006	0.2843	0.0007	0.3962	0.0009	7.187	0.072	52.72	0.53	-16.99	-0.17
2458538.88884	9.17	0.55	0.88	6.25	3.92	1.35	0.4274	0.0006	0.2881	0.0007	0.3940	0.0009	7.187	0.072	52.73	0.53	-13.79	-0.14
2458538.89512	9.60	0.58	3.08	7.81	2.33	1.11	0.4270	0.0006	0.2894	0.0007	0.3928	0.0009	7.183	0.072	52.74	0.53	-16.25	-0.16
2458538.90116	9.17	0.60	13.62	7.83	1.35	1.13	0.4272	0.0006	0.2884	0.0008	0.3924	0.0010	7.183	0.072	52.76	0.53	-17.07	-0.17
2458542.85771	4.86	0.57	-12.12	7.94	2.09	1.28	0.4293	0.0006	0.2825	0.0007	0.3909	0.0009	7.187	0.072	52.75	0.53	-17.44	-0.17
2458542.86380	4.89	0.55	-1.44	5.98	2.15	1.23	0.4290	0.0006	0.2825	0.0007	0.3908	0.0009	7.183	0.072	52.74	0.53	-16.93	-0.17
2458542.86967	5.32	0.61	-4.68	7.43	0.20	1.31	0.4291	0.0006	0.2821	0.0008	0.3918	0.0010	7.184	0.072	52.75	0.53	-19.44	-0.19
2458546.84827	4.11	0.65	10.39	8.77	-0.47	1.46	0.4270	0.0007	0.2815	0.0008	0.3780	0.0011	7.188	0.072	52.76	0.53	-15.24	-0.15
2458546.85454	3.19	0.64	9.17	9.17	1.06	1.38	0.4304	0.0007	0.2820	0.0008	0.3805	0.0011	7.188	0.072	52.75	0.53	-22.55	-0.23
2458546.85995	2.53	0.94	6.72	10.57	2.74	1.81	0.4268	0.0012	0.2815	0.0013	0.3828	0.0017	7.190	0.072	52.71	0.53	-14.24	-0.14
2458549.83603	7.59	0.74	16.37	7.77	2.73	1.62	0.4268	0.0008	0.2822	0.0010	0.3896	0.0013	7.189	0.072	52.74	0.53	-16.50	-0.16
2458549.84225	7.30	0.74	-1.73	9.74	1.57	1.59	0.4297	0.0008	0.2819	0.0010	0.3787	0.0012	7.187	0.072	52.77	0.53	-14.80	-0.15
2458549.84834	6.93	0.70	-6.41	10.41	0.43	1.22	0.4272	0.0008	0.2836	0.0009	0.3796	0.0012	7.190	0.072	52.76	0.53	-19.08	-0.19
2458565.78695	-9.61	0.54	-4.12	7.80	0.80	1.04	0.4249	0.0005	0.2841	0.0006	0.3897	0.0008	7.186	0.072	52.74	0.53	-18.58	-0.19
2458565.79317	-10.17	0.52	6.53	6.98	0.33	1.31	0.4254	0.0005	0.2834	0.0006	0.3889	0.0008	7.187	0.072	52.74	0.53	-19.36	-0.19
2458565.79932	-9.07	0.54	-5.42	7.69	2.69	1.32	0.4242	0.0005	0.2842	0.0006	0.3904	0.0008	7.188	0.072	52.73	0.53	-18.39	-0.18
2458566.74595	-6.86	0.52	-0.31	10.74	4.42	1.19	0.4272	0.0005	0.2911	0.0006	0.3906	0.0008	7.190	0.072	52.73	0.53	-18.76	-0.19
2458566.75240	-7.37	0.58	-1.78	9.82	2.28	1.34	0.4255	0.0006	0.2918	0.0007	0.3904	0.0009	7.194	0.072	52.73	0.53	-18.55	-0.19
2458566.75832	-8.57	0.55	5.99	10.45	1.07	1.19	0.4270	0.0006	0.2904	0.0007	0.3903	0.0009	7.188	0.072	52.74	0.53	-16.24	-0.16
2458567.82953	-6.61	0.64	6.09	8.03	1.89	1.15	0.4244	0.0006	0.2911	0.0008	0.3898	0.0010	7.191	0.072	52.72	0.53	-19.40	-0.19
2458567.83575	-5.46	0.68	-3.92	8.30	1.88	1.41	0.4227	0.0007	0.2916	0.0008	0.3887	0.0010	7.189	0.072	52.72	0.53	-17.08	-0.17
2458567.84185	-7.09	0.69	10.03	8.36	3.84	1.37	0.4235	0.0007	0.2907	0.0008	0.3920	0.0011	7.191	0.072	52.73	0.53	-17.86	-0.18
2458586.72225	-7.99	0.54	10.23	6.23	0.40	1.18	0.4240	0.0006	0.2854	0.0007	0.3797	0.0008	7.187	0.072	52.74	0.53	-16.84	-0.17
2458600.73936	1.78	0.64	-10.72	7.82	-0.55	1.37	0.4248	0.0006	0.2957	0.0008	0.3827	0.0010	7.190	0.072	52.74	0.53	-19.00	-0.19
2458600.74609	0.62	0.83	-7.70	8.62	-2.21	1.55	0.4236	0.0008	0.2947	0.0010	0.3827	0.0013	7.188	0.072	52.75	0.53	-17.95	-0.18
2458600.75161	2.56	0.72	11.07	7.30	-3.27	1.41	0.4246	0.0007	0.2938	0.0009	0.3827	0.0011	7.193	0.072	52.75	0.53	-19.19	-0.19
2458608.61031	11.69	0.70	-4.08	6.69	-1.13	1.47	0.4291	0.0008	0.2936	0.0009	0.3867	0.0012	7.192	0.072	52.74	0.53	-17.45	-0.17
2458608.61647	11.53	0.68	3.95	7.00	0.82	1.20	0.4259	0.0007	0.2946	0.0009	0.3891	0.0011	7.190	0.072	52.74	0.53	-19.55	-0.20
2458608.62251	10.39	0.68	11.81	7.85	-2.87	1.37	0.4265	0.0008	0.2937	0.0009	0.3875	0.0011	7.189	0.072	52.75	0.53	-14.89	-0.15
2458609.58060	11.05	0.73	6.19	7.82	-0.65	1.33	0.4251	0.0008	0.2928	0.0009	0.3856	0.0012	7.194	0.072	52.74	0.53	-20.46	-0.20
2458609.58704	10.61	0.68	11.78	7.85	0.39	1.31	0.4251	0.0007	0.2928	0.0009	0.3883	0.0011	7.191	0.072	52.74	0.53	-17.48	-0.17
2458609.59291	11.63	0.70	-3.27	7.34	-1.78	1.61	0.4241	0.0008	0.2946	0.0009	0.3883	0.0011	7.190	0.072	52.75	0.53	-14.06	-0.14
2458627.66143	10.13	0.97	-10.35	11.99	-3.93	2.08	0.4252	0.0011	0.2912	0.0013	0.3824	0.0016	7.184	0.072	52.76	0.53	-20.12	-0.20
2458627.66759	9.64	0.96	-0.22	9.40	-0.85	1.88	0.4270	0.0011	0.2899	0.0012	0.3805	0.0016	7.183	0.072	52.75	0.53	-16.45	-0.16
2458627.67363	11.91	1.01	4.34	11.17	2.58	1.99	0.4262	0.0011	0.2935	0.0013	0.3792	0.0017	7.188	0.072	52.72	0.53	-20.22	-0.20
2458667.50998	-2.86	0.64	17.00	8.56	-1.48	1.42	0.4311	0.0006	0.2916	0.0008	0.3868	0.0010	7.188	0.072	52.74	0.53	-19.73	-0.20
2458667.51614	-1.58	0.67	6.64	7.82	-0.63	1.49	0.4291	0.0007	0.2916	0.0008	0.3872	0.0010	7.188	0.072	52.75	0.53	-18.88	-0.19
2458668.48940	-2.84	0.96	-5.46	9.95	-4.90	1.96	0.4272	0.0010	0.2929	0.0012	0.3793	0.0016	7.187	0.072	52.76	0.53	-20.89	-0.21
2458668.49525	-3.53	0.91	-12.44	9.14	-2.30	1.77	0.4246	0.0010	0.2919	0.0012	0.3803	0.0015	7.190	0.072	52.75	0.53	-20.41	-0.20
2458668.50151	-1.27	0.91	3.15	9.74	-3.88	1.98	0.4302	0.0010	0.2920	0.0012	0.3795	0.0015	7.187	0.072	52.75	0.53	-17.14	-0.17

Table A3. CARMENES Doppler measurements and activity index measurements of HD 107148 in visible light.

Epoch [JD]	RV [m s ⁻¹]	σ_{RV} [m s ⁻¹]	CRX [m s ⁻¹]	σ_{CRX} [m s ⁻¹]	dLW [m s ⁻¹ * km s ⁻¹]	σ_{dLW} [m s ⁻¹ * km s ⁻¹]	H α	$\sigma_{H\alpha}$	NaD ₁	σ_{NaD_1}	NaD ₂	σ_{NaD_2}
2457768.71507	4.81	2.14	-7.07	16.03	38.79	3.51	0.4157	0.0009	0.2778	0.0014	0.3357	0.0016
2457768.72281	0.09	2.26	-17.39	17.49	48.24	3.72	0.4148	0.0009	0.2899	0.0013	0.3470	0.0015
2457813.68579	-17.68	1.29	-16.40	9.73	-15.96	1.95	0.4147	0.0006	0.2825	0.0009	0.3568	0.0010
2457813.69267	-19.87	1.31	-0.74	10.60	-10.83	1.94	0.4158	0.0005	0.2803	0.0008	0.3574	0.0009
2457813.69604	-22.99	1.16	8.53	9.16	-14.68	2.22	0.4164	0.0005	0.2804	0.0008	0.3563	0.0009
2457813.69944	-17.05	1.31	2.09	10.39	-13.12	2.22	0.4162	0.0006	0.2805	0.0008	0.3539	0.0010
2457813.70282	-19.25	1.26	-9.63	10.07	-12.95	2.32	0.4167	0.0005	0.2800	0.0008	0.3566	0.0009
2457854.54602	2.99	2.55	-1.49	20.39	5.50	4.57	0.4094	0.0010	0.2658	0.0014	0.3241	0.0016
2457854.55834	-2.69	1.87	-11.98	15.08	16.79	2.85	0.4118	0.0007	0.2834	0.0010	0.3420	0.0011
2457854.56173	4.45	1.80	16.48	14.38	15.01	2.13	0.4122	0.0007	0.2835	0.0010	0.3459	0.0012
2457854.56512	2.05	1.78	11.42	14.41	18.96	2.42	0.4122	0.0007	0.2855	0.0010	0.3459	0.0011
2457854.56849	1.20	2.06	3.69	16.60	13.49	3.13	0.4130	0.0009	0.2842	0.0013	0.3464	0.0014

Table A4. CARMENES Doppler measurements and activity index measurements of HD 107148 in near infrared.

Epoch [JD]	RV [m s ⁻¹]	σ_{RV} [m s ⁻¹]	CRX [m s ⁻¹]	σ_{CRX} [m s ⁻¹]	dLW [m s ⁻¹ * km s ⁻¹]	σ_{dLW} [m s ⁻¹ * km s ⁻¹]
2457768.71526	59.26	6.26	-5.85	33.49	41.62	5.58
2457768.72282	52.97	7.23	-4.46	39.66	32.96	4.06
2457813.68586	87.84	6.15	12.92	32.77	-4.81	5.33
2457813.69181	69.60	8.26	93.76	52.85	-27.71	7.24
2457813.69694	57.79	7.65	35.20	47.86	-22.46	4.91
2457813.70033	55.64	7.73	65.39	48.79	-18.56	6.25
2457813.70334	66.94	7.21	42.93	45.81	-30.15	6.36
2457854.54653	47.69	4.50	-18.00	24.45	22.68	3.99
2457854.55834	41.86	4.99	-1.89	28.18	6.96	3.71
2457854.56224	167.85	10.75	146.02	56.56	54.93	3.90
2457854.56613	38.49	5.07	-18.72	28.01	12.72	3.96
2457854.57002	44.64	4.83	-27.94	26.29	11.97	3.89